Keywords: phase transformation, iron mononitride, high pressure phase, *ab initio* calculations, DFT

Stability and magnetism of FeN high-pressure phases.

Alexey Kartsev,[1,2,3] Oleg Feya,[4] Nina Bondarenko,[5] Alexander G. Kvashnin,[4,6] and Artem R. Oganov[4,7,6,8]

[1)] *Computing Center FEB RAS, Khabarovsk, Russia*

[2)] *School of Mathematics and Physics, Queen's University Belfast, Belfast BT7 1NN, northern Ireland, United Kingdom*

[3)] *National Research Tomsk State University, 36, Lenina pr., Tomsk, 634050, Russia.*

[4)] *Moscow Institute of Physics and Technology, Dolgoprudny, Moscow Region 141700, Russia*

[5)] *Condensed Matter Theory Group, Physics Department, Uppsala University, S-751 21 Uppsala, Sweden*

[6)] *Skolkovo Institute of Science and Technology, 3 Nobel St., Moscow 143026, Russia*

[7)] *Department of Geosciences, Center for Materials by Design, and Institute for Advanced Computational Science, Stony Brook University, Stony Brook, New York 11794, USA*

[8)] *School of Materials Science, Northwestern Polytechnical University, Xi'an 710072, China*

(Dated: July 19, 2022)

Experimentally discovered compounds in the iron-nitrogen system belong to the low concentration part of the Fe-N phase diagram. In our paper, which is based on *ab initio* calculations we have studied formation and stability of high-pressure iron mono-nitride phases, and particularly the new magnetic phase with a NiAs-type structure. We have investigated the role of dynamic, thermodynamic and electronic properties, such as electronic correlations and pressure-induced phase stabilisation. We demonstrate that the new hexagonal FeN phase is stable for a wide range of external pressure and it can be formed as a metastable phase at zero pressure. We show that it has relativity small Curie temperature and it may possess a non-collinear magnetism.

I. INTRODUCTION

Iron and iron alloys are undoubtedly the most studied materials in the human history with the paramount importance for social and economic development. Iron nitrides are essential for a wide range of scientific and industrial applications[1]. Surface modification of iron alloys via nitrogen ions implantation is a well-established experimental technique providing the formation of surface nitrides, and therefore improving mechanical properties and increasing lifetime of these materials working under extreme conditions. The fortunate combination of magnetic properties with a high corrosion and erosion resistance have been drawing attention to these materials over the last decades. At the same time, those compounds can play an important role in addressing the geophysical issues of the meteors and planets core structure[2,3]. The nitrogen low concentration part of Fe-N phase diagram is well known and consists of several stable chemical compounds and metastable phases. Recently have been published contradictory findings about those compounds which are related to the nitrogen high concentration part of Fe-N phase diagram. In particular, a number of papers have reported the structure of the new iron mono-nitride (FeN) compounds observed in the samples prepared by sputtering ions implantation and plasma nitriding methods. Those experimental works tell us about a possible formation of two face-center cubic phases: non-magnetic γ'' - FeN with zinc blende (B3 Strukturbericht designation) structure[4–6] and magnetic rock salt (B1) structure γ'''-FeN[7,8].

From the theoretical perspective, one of the main difficulties of FeN study is*ab initio* calculations that the accurate description of transition metal compounds demands a precise accounting for electronic and magnetic effects. Therefore, a consistent study of the structural and magnetic topology of those compounds requires accurate selection of a theoretical approach [9–12] and first principles methods far beyond the standard DFT calculations. Recently, several theoretical attempts have been made to understand the crystal structure of iron mono-nitride, although there is no conclusive proof of which magnetic and structural properties belong to that phase. However, there is one important statement that most of the transition metal mono-nitrides tend to form hexagonal structures at ground state[13] or under application of pressure[14]. Taking into account this phenomenological rule, in our previous work for the first time we discovered a dynamic and thermodynamic stability of ferromagnetic $B8_1$ FeN phase[15] under high pressure which later has been confirmed experi-

mentally[16,17]. Here we present the detailed first principles analyses of FeN hexagonal phases stability in comparison with a range of high pressure FeN phases. The novel magnetic hexagonal FeN phase has been identified and its stability and magnetism at high pressures has been theoretically studied. For the sake of consistency, our results have been verified by advanced structure prediction methods using *ab initio* evolutionary techniques.[18]

II. COMPUTATIONAL DETAILS

The ground states calculations were performed using a computational implementation of the density-functional theory (DFT) package Quantum Espresso[19]. We used an ultrasoft pseudopotential approach and the Perdew-Burke-Ernzerhof (PBE) generalized gradient approximation[20] of the exchange and correlation functional within its spin-polarized version. We have employed a 600 eV energy cutoff and a 60 eV wave functions cutoff to optimize the ground state. The $24 \times 24 \times 24$ for B1 and B3 structures and $24 \times 24 \times 20$ for nickel arsenide type structure (NiAs) Monkhorst and Pack k-point meshes[21] were used for integration in the irreducible Brillouin zone by a special-points technique with broadening $\sigma = 0.02$ Ry according to the Marzari-Vanderbilt cold smearing method[22]. Thus, these meshes ensure a convergence of total energy to less than 10^{-6} eV/atom. The lattice parameters and enthalpy at finite pressure have been optimized with a variable cell-shape relaxation method. And by processing the output data from VASP the Hamilton-weighted populations were calculated based on periodic plane-wave DFT output with the aid of the 'LOBSTER' software package [23].

The vibrational properties are determined with the density-functional perturbation theory (DFPT), with vibrational spectra and the corresponding normal modes obtained from the first-principle interatomic force constants by using $6 \times 6 \times 6$ q-meshes in the first Brillouin zones within frequency convergence less then 0.5 cm^{-1}. Since the DFPT for functionals which are include Hubbard corrections not implemented into official distribution of Quantum Espresso package, we used small-displacement method[24] in order to calculate phonon spectra within GGA+U approximation.

For the purpose of thermodynamic stability verification for predicted compounds in the binary Fe-N system at a given pressure evolutionary algorithm 'USPEX' [18,25,26] has been used. We performed fixed-composition searches in the Fe-N system at pressures ranging from

0 GPa up to 60 GPa. The initial generation of 60 seed structures was created using a random symmetric generator, while all subsequent generations contained 20% random structures, 40% structures created by heredity operator, 20% by softmutation, 10% by permutation and 10% by spinmutation operators. The structural relaxations for USPEX runs were performed by using the projector-augmented wave (PAW) method in the framework of DFT, as it implemented in the VASP code[27]. The electron–ion interaction was described by means of PBE DFT functional[20] where the plane wave kinetic energy cutoff was set to 600 eV and a first-order Methfessel–Paxton smearing-function with a width δ=0.1 eV was used. Brillouin zones were sampled by Γ-centred k-points meshes with resolution $\Delta \leq 2\pi \cdot 0.07$ Å^{-1}.

Using linear-response U approach[28] for $3\times3\times3$ FeN super-cells containing j-th perturbed iron atom, an effective on-cite Hubbard interaction for i-th atom has been calculated, by taking the difference between the inverted self-consistent response matrix $\chi = \left(\frac{\partial n^i}{\partial \alpha^j}\right)_{ij}$ and the bare non-interacting response $\chi_b = \left(\frac{\partial n_b^i}{\partial \alpha^j}\right)_{ij}$: $U_i^{LR} = \left(\chi_b^{-1} - \chi^{-1}\right)_{ii}$.

Curie temperature calculations were based on DFT simulations mapped onto the Heisenberg-like Hamiltonian by calculating differences of total energies between 4 spin configurations in the extended unit cell. The magnetization as a function of temperature for Heisenberg model we calculated by using Mote Carlo method[29] in the frame of "Vampire" atomistic spin dynamics package[30]. A 50×50×50 model super-cell with periodic boundary conditions and 32,000 sites was used.

III. RESULTS

In nature, most transition metals mono-nitrides share few common crystal structures with hexagonal prototypes such as wurtzite (B4), nickel arsenide ($B8_1$) and anti-NiAs and with cubic prototypes of lattice NaCl (B1), ZnS (B3) and CsCl (B2). Usually, these compounds undergo several phase transitions from one above-named structure to another by applying external pressure[14]. They also can adopt structures which are closely related by symmetry to the discussed ones[31,32]. This fact, as a strong hint, suggested us the ability to discover a new hexagonal FeN phases formation under pressure.

In order to prove this hypothesis, we performed analysis of the total energy calculations for a number of cubic and hexagonal FeN phases at equilibrium with various configurations of the collinear spin arrangement (see Fig. 1 and supplement). It revealed that nonmagnetic B3

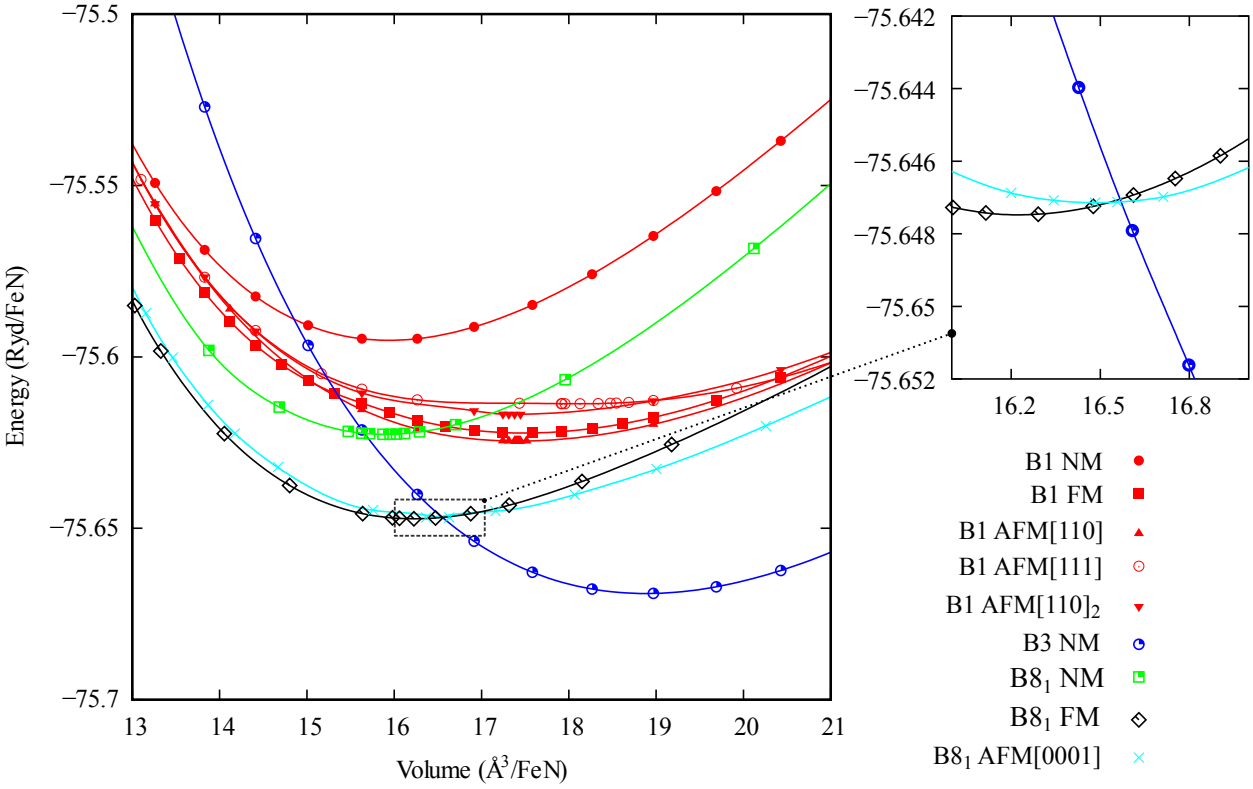

Figure 1. Calculated total energy curves as a function of unit cell volume per formula unit for different nonmagnetic (NM), feromagtic (FM) and antiferromagnetic phases. Insert correspond to the zoomed crossover area of B3 NM, B8$_1$ FM and B8$_1$ AFM[0001] phases total energy curves.

FeN is, presumably, more favoured structure at zero pressure. Converging the self-consistent calculations we observed that all collinear spin polarized solutions for zinc blende structures tend to collapse to nonmagnetic groud state, exhibiting no energy difference between the magnetic and non-magnetic B3 strukturbericht designation of FeN phases. The smallest difference of total energies at equilibrium between B3 FeN phase and others is found for non-magnetic B4 phase. So, one can suggest that the ground state for FeN should be non-magnetic B3 structure with the equilibrium lattice parameter a_{B3}=4.226 Å which is slightly smaller than the experimental values (a_{B3}^{exp} = 4.307÷4.335 Å[33–39]). At the same time, for the non-magnetic B3 phase no imaginary frequencies has been found in the phonon spectra at the experimental lattice parameter (see supplement). This check proves the coherence of the total energy and phonon spectra calculations.

Despite the fact that total energy curves for spin-polarized solutions of B1 phases lie much higher than NM B3 and FM B8$_1$ curves (see Fig. 1) meaning a larger energetic cost for the

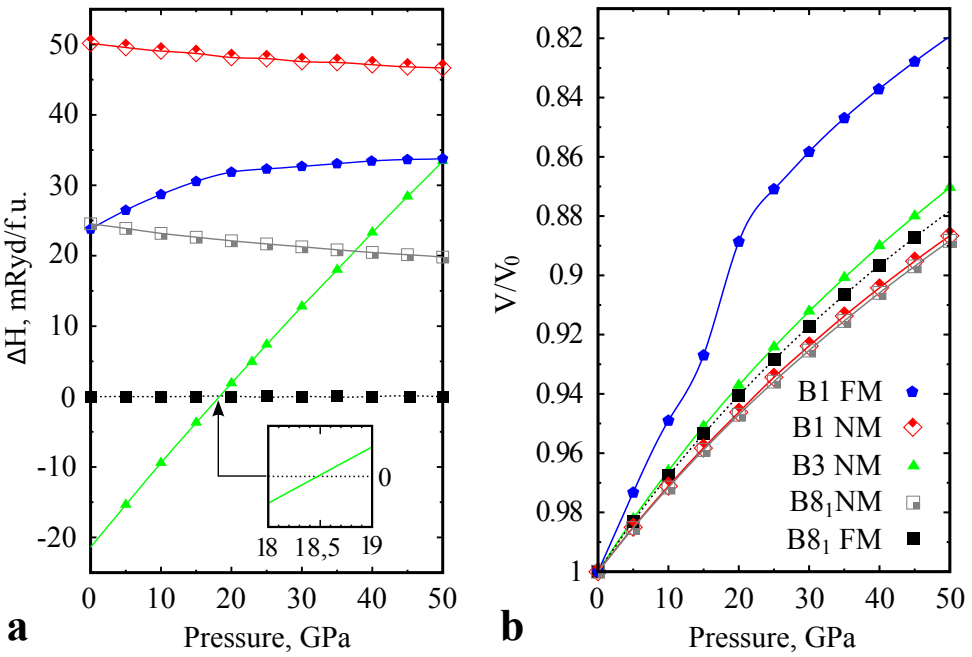

Figure 2. (**a**) Enthalpy difference as a function of pressure for different ferromagnetic (FM) and nonmagnetic (NM) FeN phases. The inset is a zoomed region which correspond to the phase transition from NM B3 to FM $B8_1$ FeN structure. The calculated value for the transition pressure turned out to be 18.5 GPa. (**b**) The normalized volume-pressure curves for non-magnetic B3, B1, $B8_1$ and ferromagnetic B1, $B8_1$ FeN phases.

B1 phase formation, such a phase has been observed experimentally[35,37] and its magnetic nature has been detected[39]. While our results for the equilibrium lattice parameters of FM B1 FeN a_{B1}^{FM}=4.119 Å and AFM[110] B1 FeN $a_{B1}^{AFM[110]}$=4.113 Å phases are in consistence with previous theoretical works[40,41]. The nature and an exact magnetic structure of B1 FeN phase is still an open question. According to our calculations the difference between FM and AFM[110] solutions at their $E^{tot}(V)$ minimums for the B1 phase is very small, therefore they are mostly discussed candidates in the literature for the collinear magnetic configuration of B1 phase[40,41]. Such a small energy difference between different magnetic configurations of B1 phase will not affect relative positions of their enthalpy and total energy curves in comparison to the magnetic $B8_1$ phases data (see Fig. 1 and Fig. 2(a)). That means that magnetic $B8_1$ phases are energetically preferable than any B1 phase and only by including correlation effects, due to their big impact on the total energy, those dispositions can be qualitatively changed. For the simplicity of comparison, only the B1 FM structure will be considered in

that paper for those results which are not taking into consideration correlation effects. The influence of electronic correlations will be discussed separately in the subsection III D.

In the same time, as you can see there is a local minimum over total energy curves in the region of values lower than the NM B3 equilibrium unit cell volume (see Fig. 1) which correspond to FM $B8_1$ FeN phase. This is our first energetic evidence for the stability of this phase under external pressure and a sign of the phase transition from B3 to $B8_1$ structure. In contrast to spin-polarized solutions of B1 structure, the energy difference between FM and AFM [0001] solutions for $B8_1$ FeN phase is noticeable enough to conclude that ferromagnetic solution is the more favourable then the AFM [0001] collinear arrangement at compressed volumes. That has been confirmed by enthalpy calculations as well (see subsection III A).

To further discuss the incompressibility of FeN phases, the evolution of their volume compression as a function of pressure is plotted in Fig 2. $P-V$ curves were calculated by optimizing the crystal structure of FeN phases under external pressures ranging from 0 to 50 GPa at 0 K without zero point energy contribution. By looking at the pressure dependence of phases unit cell volumes $P(V)$ it is evident that NM $B8_1$ is the most incompressible among considered phases (see Fig. 2(b)). The kink in the $P-V$ curve for FM B1 structure correspond to electronic spin transition to the low-spin state due to the d-orbitals nature of Fe atoms. The bulk modulus B_0 and its pressure derivative B_0' are obtained by fitting the energy-volume curve of FeN phases to the third-order Birch-Murnaghan equation of states, and they have been presented in the Table I. It is clear that the bulk modulus of FeN is larger than that for the pure BCC Fe $B_0(Fe^{BCC})$=168 GPA[42], mainly as a result of strong covalence Fe-N bonding.

A. Enthalpy calculation

The structural stabilisation of ground state phase at a certain pressure arises from the energetical interplay between different phases and it determines by Gibbs free energy. Since our DFT calculations are performed at 0 K, the Gibbs free energy becomes equal to the enthalpy and it can be defined using pressure P, total energy E^{tot} and volume V per unit cell $\Delta G(P, T=0) \equiv \Delta H(P, T=0) = E^{tot}(P) + PV$. By performing the enthalpy calculations as a function of pressure for the B3 phase and $B8_1$ phase, one can see that they have much lower enthalpy values in comparison to other cubic and hexagonal prototypes. In the

Structure	NM B1	FM B1	NM B3	NM $B8_1$	FM $B8_1$
a_0, Å	3.99	4.12	4.23	2.78	2.74
c/a	–	–	–	1.71	1.83
V_0, $Å^3$	15.9	17.5	18.9	15.9	16.2
B_0, GPa	320	180	270	330	280
B_0'	4.4	2.9	4.1	4.2	4.7
ΔH^f, mRyd	61.49	33.50	-11.74	34.07	9.66

Table I. Phases properties and characteristics at zero pressure: theoretical equilibrium lattice parameter a_0 and a/c for hexagonal structures, equilibrium unit cell volume V_0 per formula unit, bulk modulus B_0 and its pressure derivative B_0', formation enthalpy ΔH^f. per formula unit

same time, the antiferromagnetic state [0001] of $B8_1$ structure has the higher total energy (see Fig. 1) and higher enthalpy than the ferromagnetic spin arrangement for all values of external pressure with energy difference 1-4 mRyd/f.u. (starting from 1 mRyd/f.u. for 0 GPa and growing as a function of pressure up to 4 mRyd/f.u. for 50 GPa). Additionally, the entire 'zoo' of more complicated anti-ferromagnetic spin arrangements for B8 phase can be considered. And due to the relatively small energy difference between magnetic solutions, it is fair to expect for some of them to have the lower enthalpy depending on correlation effects treatment and external pressure changes. It has been confirmed by the consideration of AFM $[0001]_2$ phase - for very small pressure values around 0 GPa AFM $[0001]_2$ spin arrangement has lower enthalpy than the ferromagnetic state. Thereby it indicates a complicated character of ferromagnetic anti-ferromagnetic exchanged interplay in the magnetic $B8_1$ phase.

All of the collinear spin-polarized solutions for B1 phase energetically are even closer to each other and thereby it is hard to say which one is the most stable. Thus, taking into account an experimental fact of magnetic B1 FeN phase formation [7,8] and previous total energy arguments, we come to the conclusion that the NM B3, magnetic $B8_1$ and magnetic B1 phases are potential candidates for a high-pressure state. Using this direct method of total energies calculation it is hard to define the exact spins arrangement for B1 and $B8_1$ phases even in collinear case due to the relatively small energy difference. Thereby this question needs to be further clarified and by the use of evolutionary method we will discus

it in the following subsection IV.

At a given pressure, the most stable structure of FeN can be identified by the lowest calculated enthalpy value. Thereby transition point from one phase to another is determined by pressure value at which the enthalpies for the two different FeN phases are equal. From the Fig. 2, one can clearly see that there is a crossover which indicates a pressure-induced phase transition from NM B3 to FM $B8_1$ structure of FeN occurring at an external pressure around 18.5 GPa. On further pressure increase, the FM $B8_1$ still remain the most stable crystal configuration with decreasing magnetic moment. And therefore due to reduced impact of magnetisn to the total energy the enthalpy curve of FM $B8_1$ structure is approaching a non-magnetic solution. As you can see the crossover between B1 FM and B3 NM enthalpy curves lie much higher then transition point to the $B8_1$ phase. Phase transition to $B8_1$ is energetically much more preferable than transformation to B1 phase thereof. It has been shown by Zhonglong *et al.*[40] that maximum difference between enthalpy of B1 FM phase and other possible antiferromagnetic collinear configurations is about 10 mRyd/f.u. for the 0-50 GPa pressure range. Based on those facts we can conclude that: if we will consider total energies for the ferromagnetic and all possible antiferromagnetic structures of B1 phase and $B8_1$ phase, we will have a small difference between corresponding enthalpies values which will not affect the energetical preferability of magnetic $B8_1$ phase and the position of the phase transition point. In other words, since this point correspond to the transition from the non-magnetic B3 to the magnetic $B8_1$ FeN phase and typical exchange-magnetic energy is much smaller than enthalpy difference between magnetic $B8_1$ and magnetic B1 phases, the transition from the B3 phase to FM $B8_1$ phase will be still preferable in comparison to any other transition from the non-magnetic B3 phase to any magnetic B1 phase due to the relatively slight variation of B1 and $B8_1$ phases enthalpies with changing of their magnetic configurations. This our second evidence for the stability of FM $B8_1$ FeN phase under high pressure.

Presented total energy and enthalpy scenario lead us to controversy of FM $B8_1$ FeN phase stability to earlier findings, where pressure-induced transformation from B3 structure to B1 was indicated[10]. In fact, this kind of picture, assumes the origin of B1 phase nature to be a non pure high-pressure induced phase at low temperatures. Basically, previously B1 phase was mainly considered as a ground state of FeN at high pressures where B3 phase should undergo a phase transition. Moreover, it has been suggested as a ground state at zero

pressure[11,43] depending on the computational method and electronic correlations treatment. Only by including electronic correlations through the on-site Hubbard interaction U it is possible to turn AFM B1 phase into a ground state for some range of pressures and it will be shown further in the paper. Therefore, in concern to our results, the stability of B1 FeN phase can be seen as the temperature, electronic correlations or vacancies stabilization effects, but it can not be treated as the pure result of phase transition under external pressure like it was claimed before.

In order to evaluate the thermodynamic stability of those FeN phases, we calculated their formation enthalpies at the zero pressure and the zero temperature as follows:

$$\Delta H^f_{FeN} = H^{tot}_{FeN} - \tfrac{1}{2}H_{N_2} - H_{Fe}, \tag{1}$$

$$\frac{1}{2}N_2 + Fe \rightarrow FeN, \tag{2}$$

where H^{tot}_{FeN} represent the total enthalpy of FeN phase with FM $B8_1$, NM B3 and FM B1 structures at 0 K and at given pressure P, H_{Fe}, and H_{N_2} represent the enthalpies of bulk iron Fe with body-central cubic structure and nitrogen N_2 dimer respectively. We would like to notice that the absolute value of theoretical formation energy strongly depends on the N_2 reference phase choice and can be vary by changing of chemical potentials values. Most of the experimental studies for Fe-N phases formation at high nitrogen concentration has been performed by use of the ion implementation technique or the reactive sputtering deposition in the N_2 gas phase atmosphere. Thereof, we believe that the dimmer phase is the most appropriate choice as the nitrogen reference state.

Moreover, as shown in Table I, all ΔH^f values based on our calculations are positive except ΔH^f for NM B3 FeN phase. It is clear that formation enthalpy for the FM $B8_1$ FeN phase is much low then other positive values. Thus, other structures are metastable at ambient condition and NM B3 FeN is a stable phase. But, as it been mentioned before, those energetical dispositions can be changed by introducing electronic correlation effects into our calculations - their role in the formation energy will be discussed in the subsection III D.

B. Electronic properties and magnetism

In this subsection we present the density of states (DOS) (Fig. 4(b)), total magnetization (Fig. 4(a)) and charge density distribution (see Fig. 3 and supplement) for FM $B8_1$ FeN

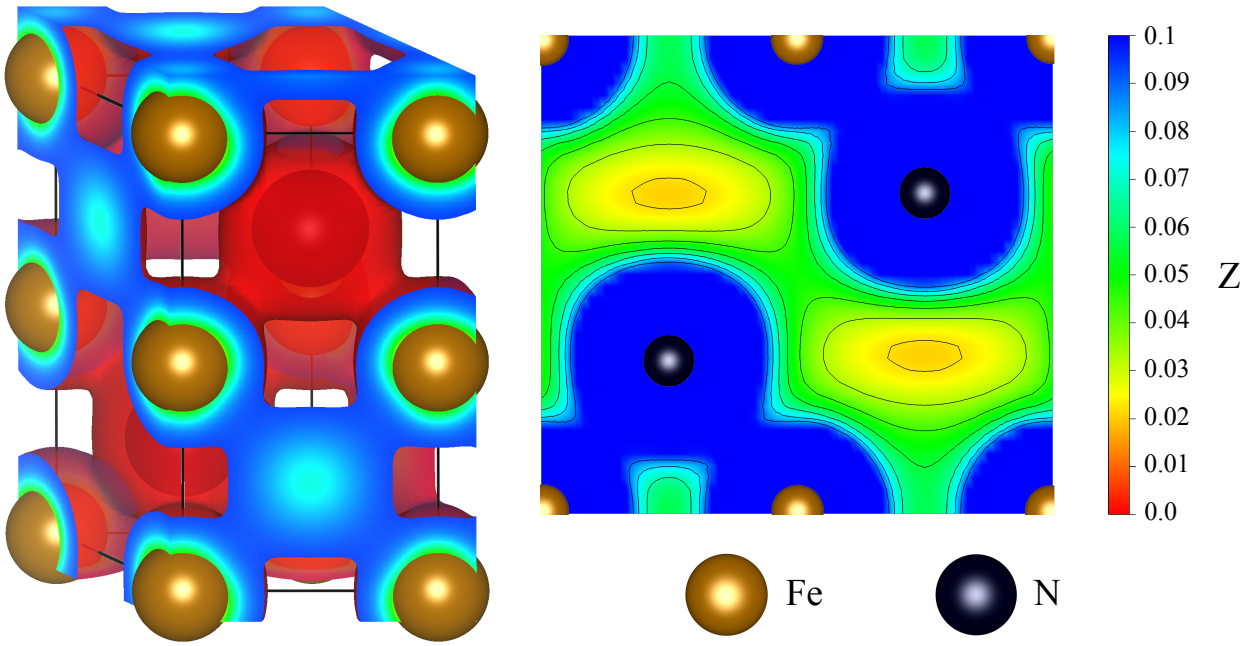

Figure 3. Three-dimensional charge density distribution in the primitive $B8_1$ FeN cell with isosurface value of 0.09 $e/Bohr^3$ and two-dimensional charge density ($0 < Z < 0.1$ $e/Bohr^3$) map in the (012) plane for ferromagnetic $B8_1$ FeN phase at P=50 GPa. Covalent interaction between Fe and N atoms is clearly visible from the localized valence electrons between the Fe and N atoms.

phase at different pressures in order to understand the origin and evolution of mechanical and magnetic properties under pressure. The charge density distribution for FM $B8_1$ FeN is shown in Fig. 3. It clearly display the formation of strong directional bonds between iron and nitrogen atoms by a strong charge accumulation between them. So, our charge density map calculations revealed the covalent nature of Fe-N bonding due to the iron and nitrogen atomic orbitals hybridisation. Furthermore, the width of covalent 'bridges' between Fe and N grow with hydrostatic pressure and this covalent nature can be confirmed by pCOHP calculation (see supplemental materials). The ionic and metallic components of chemical bond are also observed. In principle, the pressure-induced strong covalency of FM $B8_1$ FeN phase should affect the response to an isotropic compression − the crystal incompressibility, by increasing it as a function of pressure.

As shown in Fig. 4 (b), the FM $B8_1$-FeN phase along with covalency FM exhibit obvious metallic characteristics with the finite DOS at the Fermi energy level at all pressures. A strong hybridisation between metal d electrons and nonmetal p electrons which correspond to the strong Fe-N covalent bonding is observed as well(see Fig. 5). With the pressure

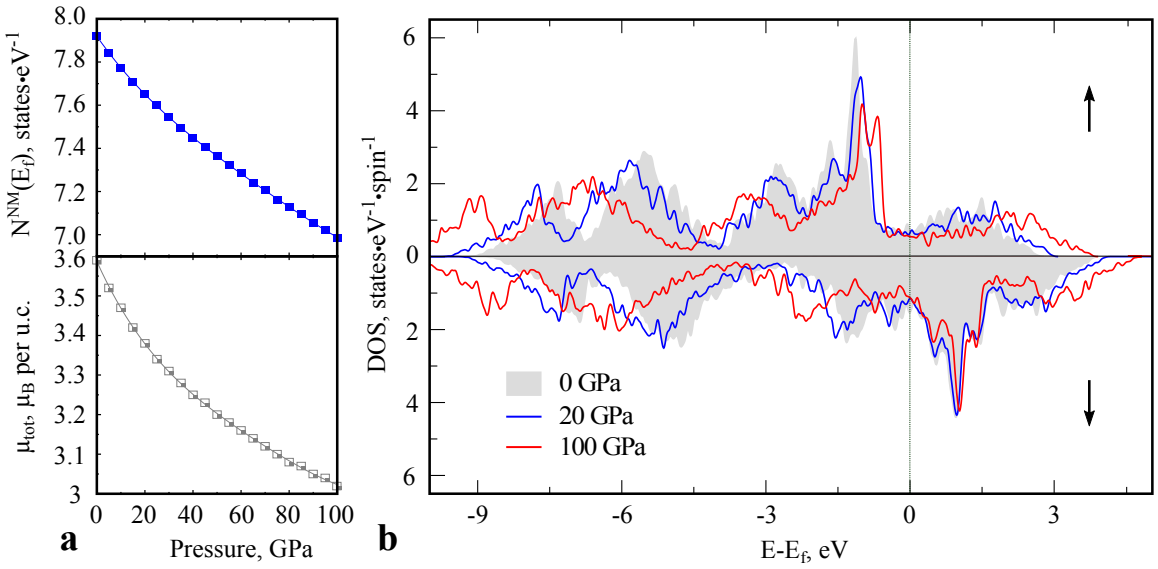

Figure 4. (**a**) Density of states at Fermi level ($N^{NM}(E_f)$) for non-magnetic $B8_1$ FeN phase and total magnetic moment μ_{tot} of ferromagnetic NiAs FeN phase per unit cell (which contain 2 Fe and 2 N atoms) containing 4 atoms as a function of pressure. (**b**) Density of electronic states (up and down channel) for ferromagnetic $B8_1$ FeN phase at different pressures. The position of Fermi level (E_f) as reference energy is defined as zero.

increase, DOS peaks of $p-d$ bonding and $p-d$ anti-bonding states slightly move to left direction. This shift forces electrons to occupy more bonding states, which enhance the covalent bonding and phase structural stability thereof. Moreover, compared to a 0 GPa state the DOS distribution under pressure is more broadened, but in the same time the Fermi level keeps its position in the valley and the DOS value at Fermi energy stay almost invariably, therefore this also indicates stability of an electronic structure.

For the itinerant electron model of ferromagnetic phase competing with non-magneitc phase, as pressure increase, magnetic moment (μ_{tot}) and effective density of states of the corresponding paramagnetic phase tend to decrease due to the band widening[44]. In the framework of Stoner model, assuming that effective Stoner parameter is a constant, the instability criterion for paramagnetic phase is $I \cdot N^{NM}(E_f) > 1$, there I is Stoner effective exchange parameter with typical value corresponding to d electrons of iron I=0.63-0.98 eV/states [45,46] and N^{NM} is an effective density of states corresponding to paramagnetic phase. In other words, according to the Stoner model in the framework of classical band theory, as pressure is increased the effective density of states N^{NM} should be decreased.

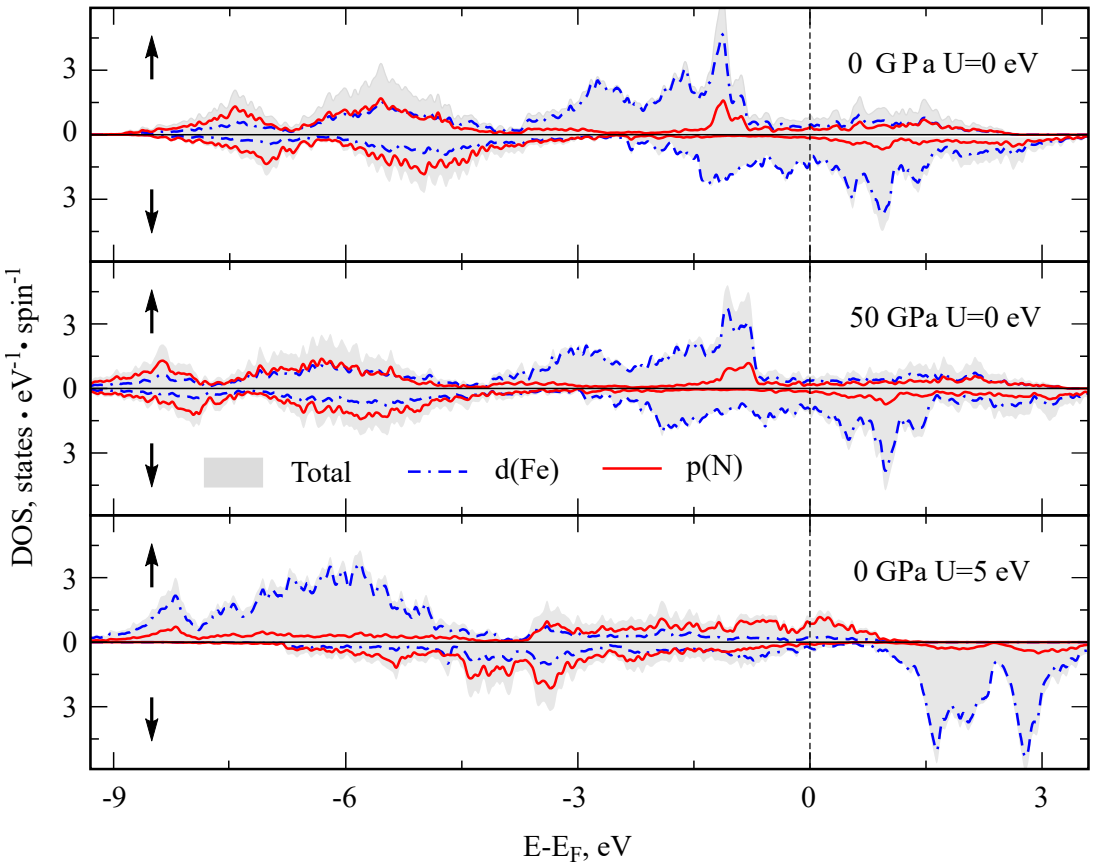

Figure 5. Density of electronic states and partial density of states (up and down channel per 2 Fe/N-atoms) for ferromagnetic $B8_1$ FeN phase at 0 GPa, 50 GPa pressures and 0 GPa pressure with on-site Hubbard $U = 5$ eV . The position of Fermi level (E_f) as reference energy is defined as zero.

Thereby band ferro-magnetism in the system damps under external pressure and eventually disappear at some critical point. Taking the DFT non-spin-polarized solution as a mean-filed approximation for paramagnetic state, the capacity of Stoner model to describe magnetism of the FM $B8_1$ phase is well supported by our calculations of effective DOS at Fermi level and total magnetic moment per unit cell of the FM $B8_1$ FeN phase (see Fig. 4 (a)) – the number of effective states at Fermi level $N^{NM}(E_f)$ of non-magnetic phase drops down as a function of pressure and the total magnetisation of FM phase falls with pressure thereby. It is obvious that electronic structure of NM $B8_1$ FeN phase should satisfy to the Stoner instability criteria of paramagnetic solution for a quite broad range of pressures.

Furthermore, based on the Heisenberg-like model we performed estimation of the Curie temperature using the Monte Carlo simulations[29] for FM $B8_1$ phase. By fitting Monte-Carlo

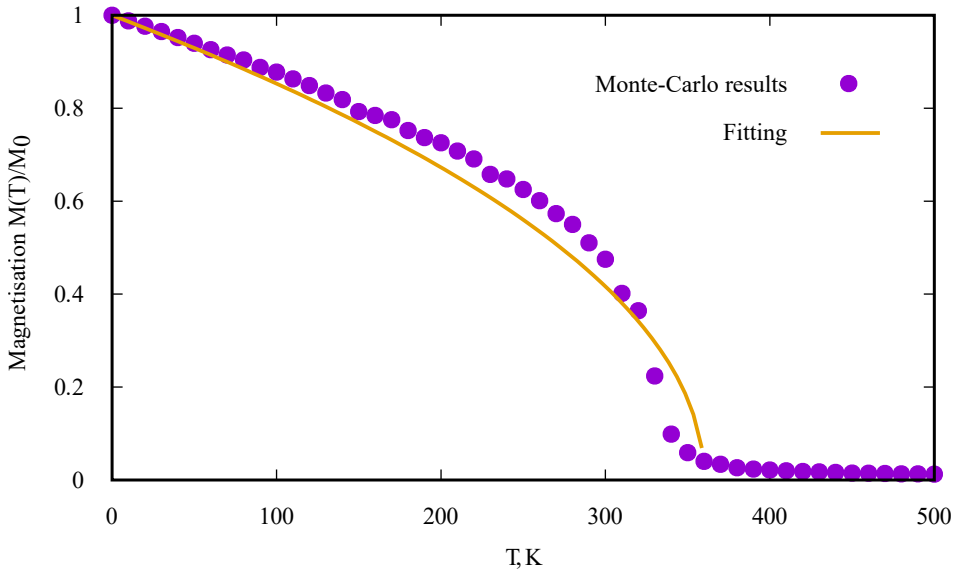

Figure 6. Monte Carlo simulation of temperature-dependent magnetization for FM $B8_1$ FeN phase. The temperature-dependent magnetization is fitted to the expression $M^f(T)/M_0 = (1 - T/T_c)^\beta$ (shown by the solid line) which yields a fitted $T_C \approx 620$ K and exponent $\beta \approx 0.47$.

results (see Fig. 6) with the following function $M^f(T) = M_0 \cdot \left(1 - \frac{T}{T_c}\right)^\beta$ we obtained the Curie temperature $T_C \approx 360 - 380$ K for the $0 - 50$ GPa range of external pressure and the critical exponent $\beta \approx 0.49$ (see supplement materials for details).

C. Dynamic properties

In this section, we study the phonon spectra of FM $B8_1$ FeN phase, where the absence of soft modes can serve as the main evidence of the crystal structure stability. Our phonon calculations based on the DFPT performed at different pressures confirm the dynamic stability of FM $B8_1$ FeN phase (see Fig. 7). The dynamic stability of FM $B8_1$ FeN structure is observed even at zero pressure (see Fig. 7). This fact asserts our suggestion that the FM $B8_1$ FeN phase can manifest stability even at low pressure as a metastable structure depending on the activation conditions. Furthermore, computed phonon dispersion curves for the first Brillouin zone show the pressure enhanced dynamic stabilisation and no sign of modes softening against hydrostatic pressure from 0 GPa till 100 GPa. The phonon frequencies increase with pressure and this effect induced due to the strength of covalent Fe-N bonds at

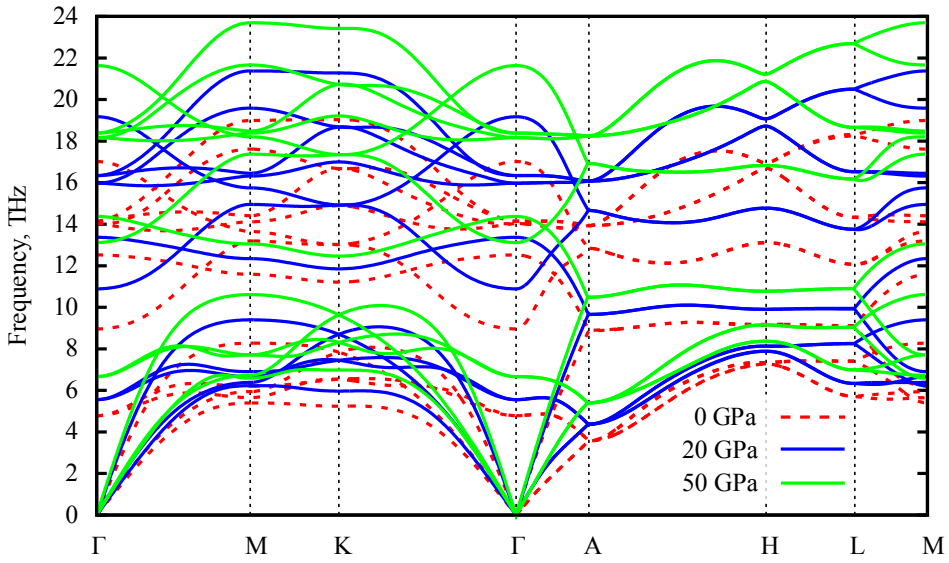

Figure 7. Phonon dispersion curves for FM $B8_1$ FeN at 0 GPa (dashed red line), 20 GPa (solid blue lines) and 50 GPa (solid green lines).

high pressure: pressure-induced accumulation of charge in the Fe-N direction (see subsection III B) lead to the more pronounced covalent character of Fe-N bonding, therefore stronger covalent Fe-N bonds with decreased length enhance phonon modes.

The total phonon DOS of FM $B8_1$ phase, as well as the projected DOS for Fe and N atoms obtained by the DFPT, are shown in Fig. 8. For the acoustic part of phonon DOS, we can see the major contribution of Fe vibrations due to the large atomic masses difference between Fe and N. Thereby, partial DOS indicate a low Fe-N phonon hybridization degree and weak contribution of Fe to the optic part. The shapes of the phonon DOS curves for the 0-50 GPa range of pressures are rather similar. By further increasing external pressure the degree of hybridization between acoustic and optical modes decrease and lead to the phonon band gap opening at pressure value $P_g \gtrsim 50$ GPa. Using quasi-harmonic approximation[47] for FM $B8_1$ FeN phase at equilibrium unit cell volume the ground state Debye temperature is found to be $\Theta(T = 0) \approx 850$ K and $\Theta(T = \infty) \approx 710$ K for the high-temperature limit[15], which is almost twice higher than it is for the cubic iron[48] and for the hexagonal phase of iron[49].

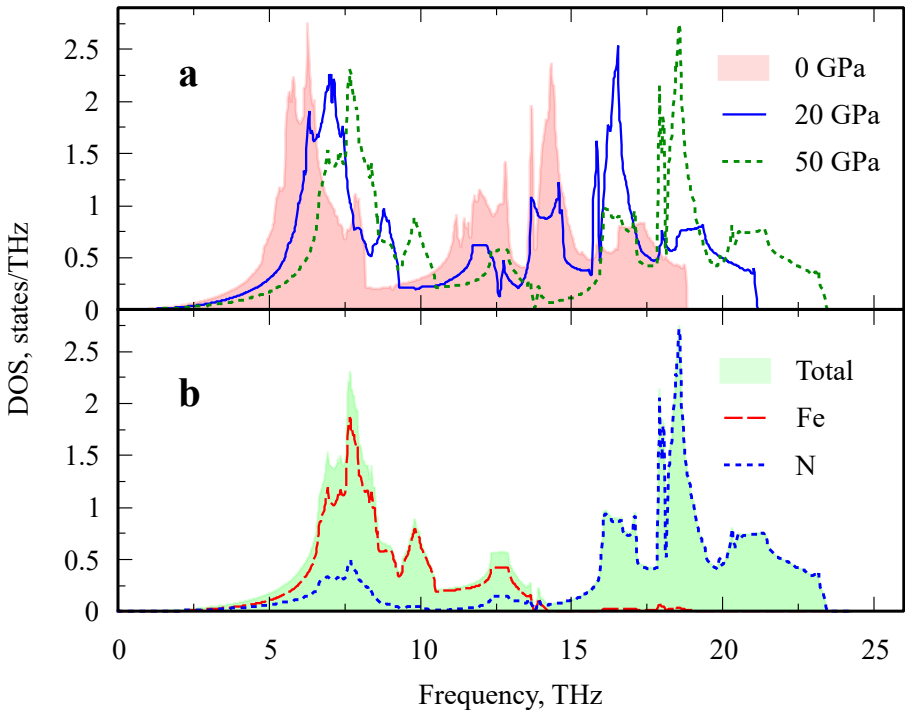

Figure 8. **(a)** Phonon density of states at 0 Gpa, 20 GPa and 50 GPa for ferromagnetic NiAs-FeN phase at zero temperature. **(b)** Total (4 atoms/unit cell) and partial phonon (per 2 Fe/N-atoms) density of states at 50 GPa.

D. Influence of electronic correlations

It has been recently shown that for the ground state of transition *d*-metals mononitrides[50–52], and particularly for iron mononitrides[40], electronic correlations can play a crucial role in the phase stabilisation. In order to understand the impact of electronic correlations to the $B8_1$ phase stability, we performed a GGA+U calculation for the enthalpy and total energy as a function of on-site Hubbard U repulsion for electronic states of localized Fe d orbitals[53]. As you can see from the Fig. 9, by introducing on-site Hubbard correction U, we do not change the prefavrouble phase at high pressure due to the enthalpies-pressure dependence. In the same time, another unknown phase may appear to be more energetically preferable and we will discus that further in the paper. So, we can conclude that energetic favorability of FM $B8_1$ against NM B3 configuration of FeN at high pressures remains actual despite to including correlation effects vi Hubbard term. Moreover, for $U \gtrsim 3.5$ eV the ground state structure at zero pressure is the magnetic $B8_1$ phase. This is the sign of the

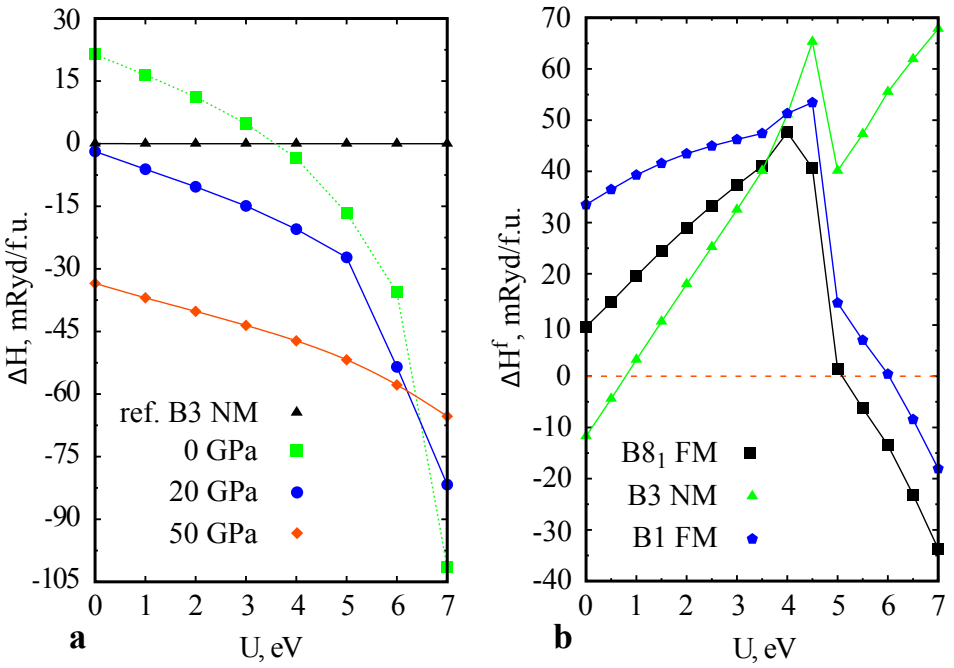

Figure 9. (**a**) Enthalpy difference of ferromagnetic $B8_1$ FeN phase as a function of on-site Hubbard repulsion U at different pressures. Enthalpy for non-magnetic B3 FeN phase was taken as a reference points at each corresponding value of pressure and U. (**b**) Formation enthalpy as a function of on-site Hubbard repulsion U for non-magnetic B3 and ferromagnetic B1, $B8_1$ FeN phases.

strong structural dependence of FeN on the electronic correlations at zero pressure and this result is in line with the previous calculations[40].

Another thermodynamic quantity which has been analysed respectively to the correlation effects influence is the phases formation energy at $P = 0$ GPa from the N_2 gas phase and BCC Fe. The effect of introducing Hubbard U for d orbitals on the FeN formation enthalpy in the reaction (2) is rather controversial - it make the NM B3 FeN phase less stable at zero pressure compare to other phases and turn the reaction of its formation for $U \gtrsim 1.0$ eV to endothermic one, in other hand for a relativity big values of U formation reactions of $B8_1$ FM and B1 FM FeN phases are exothermic processes due to the magnetic transition in FeN compounds from the low- to the high-spin states.

Talking about the impact of electronic correlations to electronic, magnetic and structural properties, one can notice specific jump in $a_0(U)$, $c_0(U)$ and $\mu(U)$ curves which correspond to the spin state transition from a low-spin state to a high-spin state of iron d electrons (see Fig. 10) like it is in the previous case of formation enthalpy curve. In general, both for

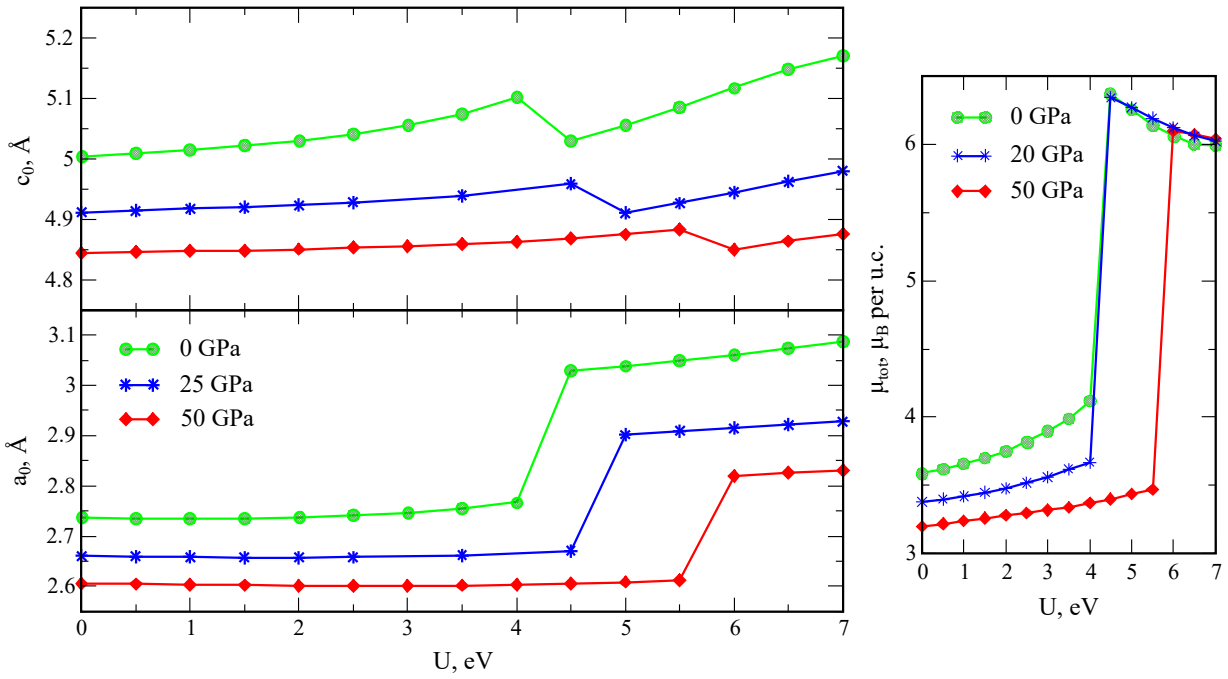

Figure 10. Lattice parameters and total magnetic moments per unit cell (2 Fe and 2 N atoms) at different hydrostatic pressures as a function of on-site Hubbard repulsion U for ferromagnetic $B8_1$ FeN phases.

lattice parameters and for total magnetic moments curves a growing character as a function of on-cite Hubbard repulsion U can be notice at the low-spin state region. In the same time, according to our results of charge density calculations the including of correlation effects by introducing Hubbard U weakly affect the width of $Fe-N$ covalent bridges on the charge density map and thereof has no strong impact to the covalent character of $F-N$ bonds.

Another strongly U-dependent quantities are found to be magnetic exchanges, magnetic anisotropy and Curie temperature. While in the case of $U \lesssim 1$ eV the FM solution for $B8_1$ phase is found to be more favourable then NM and AFM [0001] at the 0-100 GPa pressure range, by including the Hubbard U into our calculation the AFM exchange is dominated. And therefore the preferable magnetic order can be switched to the AFM[0001] configuration or to the AFM$[0001]_2$ where the spin configuration is arranged by double spin layers altering along the z-axis. (see supplement materials). So the competition of FM and AFM exchanges in the magnetic $B8_1$ has a complicated character and strongly depends on the electronic correlations.

In order to investigate the impact of electronic correlations onto dynamic stability of

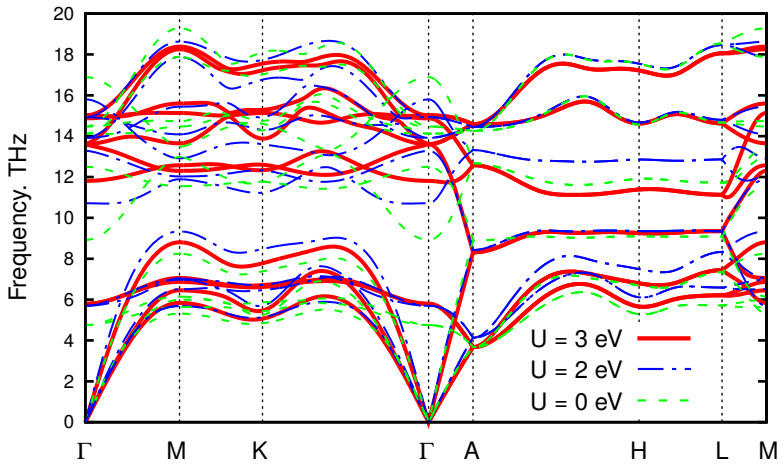

Figure 11. Phonon spectra for ferromagnetic $B8_1$ FeN at zero pressure using GGA+U approach for different values of the Hubbard on-site: green dashed curves are $U = 0$ eV, blue dashed curves are $U = 2$ eV and thick red curves are $U = 3$ eV.

FM $B8_1$ FeN phase, we performed phonon calculations at zero pressure by use of GGA+U calculations (see Fig. 11). We found that phonon dispersion of FeN $B8_1$ persists dynamic stability against electronic correlations included via Hubbard term U in the framework of DFT+U formalism. Since the DFPT for functionals which contain Hubbard term not implemented into the official distribution of Quantum Espresso package, we have to use a small-displacement method in order to perform DFT+U phonon calculations. Unfortunately, for $U > 3$ eV we were not able to converge self-consistent calculations for some distorted supercells due to the large d orbitals deformation.

Additionally to our simulations, using linear-response method we estimated values of Hubbard U^{LR} acting on iron d-orbitals for three main phases at zero pressure. However, the DFT+U^{LR} values corresponds to a mean-field solution of the quantum impurity problem in the frame of dynamical mean-field theory. In general, this Hartree-Fock solution tends to overestimate interactions effects. Thereby in order to get a correct description of interactions effects, the employed U value should be smaller than what we get out of the linear response U^{LR}. We found that effective $U^{LR}(Fe)$ is equal to 4.3 eV, 6.7 eV and 2.7 eV for d electrons of FM $B8_1$, NM B3 and FM B1 FeN phases at zero pressure respectively. These values fall into the range of U values we explored. In other hand, comparison to experimental results for magnetic moment measurements $\mu_{exp} \approx 3.4\mu_B$[16] suggest us the low-spin state

in the magnetic $B8_1$ FeN phase. Thereby the reasonable value of $U \approx 3$ eV should reflect correct properties of that phase and correspond to very small enthalpy difference between NM B3 and FM $B8_1$. It means that the B3-$B8_1$ phase transition should undergo at much low than previously defined transition pressure 18.5 GPa and correlations effects can lead to the metastable character of FM $B8_1$ phase at zero pressure. And in fact, this phase was observers experimentally at $P = 0$ GPa by the quenching to ambient pressure[16].

In principle, in order to have a full understanding of the electronic correlations impact on FeN properties, we should calculate the Hund's rule coupling J, which is particularly crucial to describe the ground state of systems with a non-collinear magnetism. Moreover, the Hubbard U is different for each d-orbital, changes with pressure and should be found self-consistently using an infinite super-cell. Thereby, obtained numbers for such a complex system are rather estimations of the highest boundary of U value and indicate that electronic correlations have a quite noticeable character for the FeN phases formation. So, taking in account previous arguments, we can say that their impact on stability can change a lot from phase to phase and should be considered as one of the most critical parameters.

E. Non-collinear spin structure

It should be noted that other compounds of $3d$ metals with a small energy difference between various spin configurations can exhibit a non-collinear magnetic structure. Thereof, a theoretically obtained spin arrangement for those compounds is very sensitive to computational approaches and to the correlations treatment. Non-collinear magnetism can arise naturally due to the geometric frustration of AFM interactions or due to the magnetic anisotropy. In turn, in the $B8_1$ FeN structure along the [0001] plane a triangular structure of Fe atoms can be found and thereby due to the geometric frustration this triangular arrangement of magnetic atoms can exhibit a non-collinear magnetic structure. Moreover, there is no deep experimental investigation has been concentrated on magnetic properties of NiAs-type FeN. A layered stacking of iron atoms in the hexagonal $B8_1$ FeN phase is highly likely will lead to exotic magnetic properties, similar to the spin-spiral arrangement in the covalent iron and chromium chalcogenides and pnictides with $B8_1$ structure[54–56]

In this paper, due to the limitations of our computational tools, we performed calculations mainly for collinear magnetic solutions. For the test purpose, we performed relaxation of $B8_1$

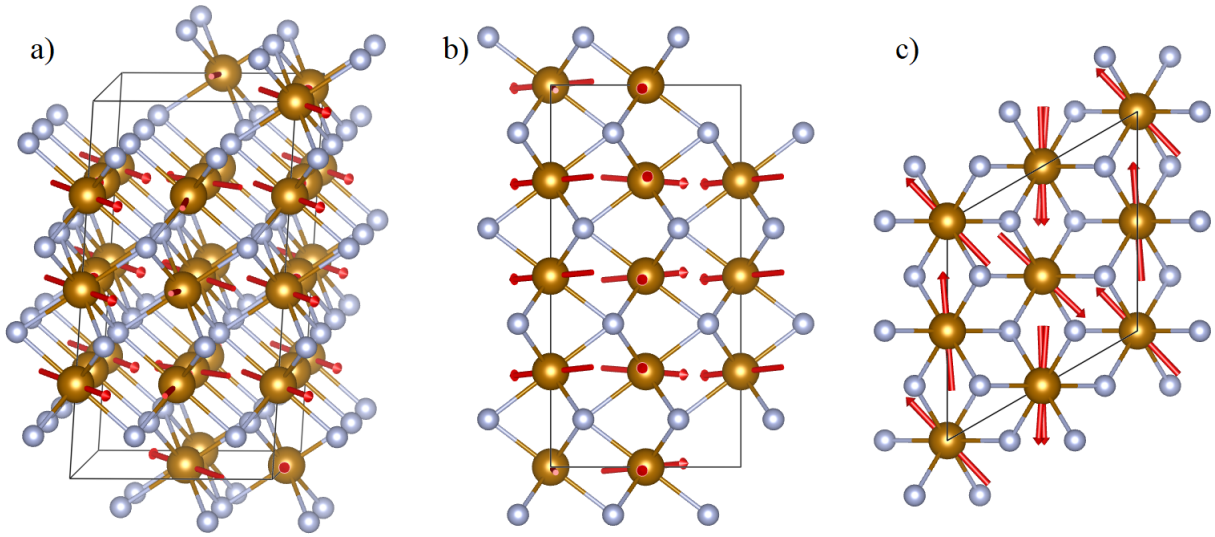

Figure 12. Relaxed non-collinear spin structure of FeN $B8_1$ 2×2×2 supercell with the Hubbard on-site repulsion $U = 6$ eV. Side-views a), b) and top-view c). Red arrows correspond to the local magnetization direction of Fe-atoms with magnetic moments equal to 4.03 μ_B. Large goldish balls denote iron atoms and light blue balls denote nitrogen atoms.

FeN structure with few random non-collinear spin structures using VASP. We found that for some values of U relaxed structures with non-collinear spin configurations are energetically preferable than the collinear ferromagnetic state. For example, using 2×2×2 supercell of $B8_1$ FeN and by fixing pressure $P = 0$ GPa and values of U equal 6 eV and 4 eV for d-orbitals we found relaxed structures with a non-collinear spin configurations which have a lower total energy by 50.4 mRyd and 16.5 mRyd per structural unit cell (2 atoms of Fe and 2 atoms of N) than the ferromagnetic configuration (see Fig. 12).

IV. EVOLUTIONARY ALGORITHM PREDICTIONS. USPEX PART

In order to verify our results and validate the FeN $B8_1$ phase stability at high pressure by the independent method we have used VASP code in the framework of evolutionary algorithm 'USPEX'. Thereby, using 'USPEX' code a stable structure search was performed at the following fixed values of external pressure P - 0 GPa, 20 GPa, 40 GPa and 60 GPa. For a better understanding of the electronic correlations impact to structural stabilities at 0-50 GPa pressures range we performed these calculations for two fixed values of on-site

Table II. The most stabel structures obtained by the evolutionary method for values 0 eV and 4 eV of on-site Hubbard correction U and 0 GPa, 20 GPa, 40 GPa and 60 GPA of external pressure P with corresponding symmetry groups. For enthalpies difference ΔH configuration with a lowest value of H chosen as a reference state for the each case of P and U combination. μ_{Fe} is the value of magnetic moment on the iron atom. a_0 is the lattice parameter (for a full description of non-cubic structures please see the supplement material)

P, GPa	U, eV	Symmetry	Magnetism (μ_{Fe}, μ_B)	ΔH, mRyd/FeN	V_0, Å^3	a_0, Å	Composition
0	0	216 (B3)	NM	0.0	18.9	4.21	2-2
0	0	44	NM	1.32298	18.9	2.97	3-3
0	0	186 (B4)	NM	17.75727	19.0	2.93	4-4
0	0	194 ($B8_1$)	FM (1.6)	28.70856	16.2	2.73	2-2
0	0	225 (B1)	FM (2.11)	57.15253	16.8	4.06	5-5
0	4	216 (B3)	AFM (3.83)	0.0	23.3	4.44	4-4
0	4	186 (B4)	FM (3.87)	2.08736	23.5	5.24	4-4
0	4	160	AFM (3.85)	3.49853	23.3	5.47	4-4
0	4	194 ($B8_1$)	AFM (3.89)	6.49728	22.5	5.53	4-4
0	4	186 (B4)	AFM (3.90)	10.99539	23.8	3.24	4-4
0	4	225 (B1)	AFM (3.93)	13.02396	19.5	3.01	4-4
20	0	82	NM	0.0	17.3	4.07	5-5
20	0	44	NM	1.45527	17.3	2.74	3-3
20	0	216 (B3)	NM	3.21924	17.8	2.92	2-2
20	0	194 ($B8_1$)	FM (1.49)	6.39438	15.2	2.67	2-2
20	0	186 (B4)	NM	22.16718	18.0	2.95	2-2
20	4	225 (B1)	AFM (3.89)	0.0	18.0	5.07	4-4
20	4	194 ($B8_1$)	AFM (3.72)	4.76271	17.7	2.85	4-4
40	0	194 ($B8_1$)	FM (1.41)	0.0	14.5	2.62	2-2
40	0	62	AFM (1.42)	2.52835	14.6	4.8	4-4
40	0	216 (B3)	NM	19.25664	17.0	2.88	2-2
40	4	225 (B1)	AFM (3.84)	0.0	17.0	2.87	4-4
40	4	194 ($B8_1$)	AFM (3.58)	1.44057	16.4	2.76	4-4
40	4	225 (B1)	FM (3.08)	8.96683	16.6	2.86	2-2
60	0	194 ($B8_1$)	FM (1.38)	0.0	14.0	2.59	2-2
60	0	62	AFM (1.51)	3.01344	14.0	4.55	2-2
60	0	187	FM (1.67)	12.87696	14.0	2.58	3-3
60	4	194 ($B8_1$)	AFM (1.61)	0.0	14.1	2.61	2-2
60	4	225 (B1)	AFM (2.89)	2.13146	15.2	2.8	2-2

Hubbard interaction U - 0 eV and 4 eV.

We have summarized obtained results into the table II where thermodynamically most stable structures are listed. For $P = 0$ GPa and $U = 0$ eV we were able to get all structures mentioned above in that paper. And then the most stable phase is a non-magnetic FeN B3.

While for $U = 4$ eV this phase becomes an anti-ferromagnetic. For $P = 20$ GPa and $U = 0$ eV we discovered a new FeN phase with symmetry 82 to be the most stable one. While by the including electronic correlations with Hubbard $U = 4$ eV the most stable phase is a anti-ferromagnetic B1 structure which is energetically very close to the anti-ferromagnetic $B8_1$ FeN phase. With further pressure increase up to 40 GPa, we got a ferromagnetic $B8_1$ FeN phase as the most stable one for $U = 0$ eV and anti-ferromagnetic B1 FeN for $U = 4$ eV competing with anti-ferromagnetic $B8_1$ FeN phase. At the highest pressure we concerned - P =60 GPa, the ferromagnetic $B8_1$ FeN phase is the most stable one for U=0 eV, while by putting Hubbard U =4 eV, the AFM configuration gains the stability. Based on those results we can conclude that effect of correlations can change drastically phase stability which is in the consistent with our previous findings (see section III D).

Obtained results based on the evolutionary algorithm fully support our phenomenologically based idea of magnetic $B8_1$ FeN phase stability. The only difference we found is that due to correlation effects for some values of Hubbard U and small range of the external pressure the different phase is energetically more preferable. For example, for $U = 4$ eV and $P \approx 20 - 40$ GPa the ground state found to be AFM B1 structure. Since stabilization of this phase is possible only at certain pressures and specific values of U, it does not controvert our previous findings and can be addressed as an important issue for the future research. Another an important issue is proved - $B8_1$ FeN phase can exhibit an anti-ferromagnetic arrangement of spins depending upon the correlations treatment, while experimentally only FM ordering been suggested for $B8_1$ FeN structure[16].

V. CONCLUSION

Concluding our work which is based on DFT calculations, the FeN is observed to exhibit a pressure induced structural transformation from the low-pressure cubic B3 structure to the high pressure hexagonal $B8_1$ structure. Based on our calculations, we propose that the $B8_1$ is a high-pressure magnetic phase of FeN, as this phase has the lowest total energy per unit cell among others at suppressed volumes and shows dynamic stability with a wide range of external pressure. We have explored the structural, electronic and magnetic properties of the hexagonal NiAs-type FeN phase under the high pressure and we found it as a strong covalent material with high magnetic moment persistence against pressure. The value of

transition pressure from nonmagnetic ZnS to the FM $B8_1$ phase is determined to be 18.5 GPa.

Calculated total energy difference between collinear FM, AFM and non-collinear magnetic solutions for $B8_1$ FeN phase is very small and it depends upon to the correlations treatment and external pressure. Thereof it is impossible to define its exact magnetic structure. The only clear conclusion which can be brought here is that $B8_1$ FeN phase is magnetic with possibly more complicated spin structure than just a collinear ferro-magnetism. Moreover, this phase exhibit a strong magnetic exchange upto $T_C \approx 360K$ and it can be formed as a bulk sample at 0 GPa due to it metastable nature. Thereby, this material looks very promising for a wide range of real applications. Moreover, it can serve as one of the main candidates for planets inner core magnetic materials with a relatively high total magnetic moment per unit cell at high pressures and temperatures.

Our first principles study will help to extend the fundamental knowledge of Fe-N phase diagram. It has clearly identified the stability of magnetic high pressure $B8_1$ phase of FeN, controversially to the previously claimed phase transition of FeN to NaCl-type structure under high pressure. To the best of our knowledge, our work is the first theoretical projection on the properties ans stability of FeN magnetic high pressure hexagonal phase.

Since the iron-rich core of meteors and Earth can contain a sufficiently big amount of light elements including nitrogen[2,3] the problem of iron nitrides formation at non-standard conditions is actual for astronomy and geoscience. Therefore as an application aspect, it is important to understand magnetic properties of the new phase at high temperature and pressure. At Ref.[57] it has been shown that due to the spin fluctuations even under the Earth's core conditions Fe acquires substantial local magnetic moment. It can thus be suggested that iron nitrides can exhibit magnetism under extreme conditions too. A further study with more advanced finite-temperature methods and non-collinear techniques is therefore suggested, where some messages to the physics of magnetism and astrogeology issues can be addressed.

VI. SUPPLEMENT MATERIAL

See supplement material for complete $E(V)$ curves for all considered phases, the charge density of FM $B8_1$ FeN phase evolution under pressures, density of states for non-magnetic

B8 1 FeN phase, phonon dispersion curve for NM B3 FeN phase, calculated crystal orbital Hamilton population (-COHP) for FM, AFM$[0001]_1$ and AFM$[0001]_2$ $B8_1$ FeN phases, details of magnetic exchanges and critical temperature calculation for FM $B8_1$ FeN phase and magnetic anisotropy calculations. It also includes calculations of magnetic exchanges and Curie temperatures at different pressures and for different on-site Hubbard U values.

VII. ACKNOWLEDGEMENT

The study was carried out with the partial support of the RFBR grant No. 18-29-03196. Data processing was performed using the Shared Facility Center resources "Data Center of FEB RAS" (Khabarovsk)[58].

REFERENCES

[1]C Navío, J Alvarez, MJ Capitan, J Camarero, R Miranda, et al. Thermal stability of cu and fe nitrides and their applications for writing locally spin valves. *Applied Physics Letters*, 94(26):263112, 2009.

[2]Jennifer F. Adler and Quentin Williams. A high-pressure x-ray diffraction study of iron nitrides: Implications for earth's core. *Journal of Geophysical Research: Solid Earth*, 110(B1), 2005. B01203.

[3]Sayuri Minobe, Yoichi Nakajima, Kei Hirose, and Yasuo Ohishi. Stability and compressibility of a new iron-nitride β-fe_7n_3 to core pressures. *Geophysical Research Letters*, 42(13):5206–5211, 2015. 2015GL064496.

[4]Cristina Navio, Jesus Alvarez, Maria Jose Capitan, Felix Yndurain, and Rodolfo Miranda. Nonmagnetic γ''-fen thin films epitaxially grown on cu(001): Electronic structure and thermal stability. *Phys. Rev. B*, 78:155417, Oct 2008.

[5]X. Wang, W.T. Zheng, H.W. Tian, S.S. Yu, W. Xu, S.H. Meng, X.D. He, J.C. Han, C.Q. Sun, and B.K. Tay. Growth, structural, and magnetic properties of iron nitride thin films deposited by dc magnetron sputtering. *Applied Surface Science*, 220(1–4):30 – 39, 2003.

[6]C Navio, M J Capitan, J Alvarez, R Miranda, and F Yndurain. Formation of a nonmagnetic metallic iron nitride layer on bcc fe(100). *New Journal of Physics*, 12(7):073004, 2010.

[7]Toru Hinomura and Saburo Nasu. A study of fe–n alloy systems. *Hyperfine Interactions*, 111(1-4):221–226, 1998.

[8]L Rissanen, M Neubauer, K.P Lieb, and P Schaaf. The new cubic iron-nitride phase fen prepared by reactive magnetron sputtering. *Journal of Alloys and Compounds*, 274(1–2):74 – 82, 1998.

[9]A. Houari, S.F. Matar, and M.A. Belkhir. Ab initio investigation of the electronic structure and the magnetic trends within equiatomic fen. *Journal of Magnetism and Magnetic Materials*, 312(2):298 – 304, 2007.

[10]Pavel Lukashev and Walter R. L. Lambrecht. First-principles study of the preference for zinc-blende or rocksalt structures in fen and con. *Phys. Rev. B*, 70:245205, Dec 2004.

[11]Y Kong. Electronic structure and magnetism of equiatomic fen. *Journal of Physics: Condensed Matter*, 12(18):4161, 2000.

[12]A. Filippetti and W. E. Pickett. Prediction of a ferromagnetic ground state for nacl-type fen. *Phys. Rev. B*, 59:8397–8400, Apr 1999.

[13]Jiaqian Qin, Xinyu Zhang, Yanan Xue, Xinting Li, Mingzhen Ma, and Riping Liu. Structure and mechanical properties of tungsten mononitride under high pressure from first-principles calculations. *Computational Materials Science*, 79:456 – 462, 2013.

[14]R. Rajeswarapalanichamy, G. Sudha Priyanga, M. Kavitha, S. Puvaneswari, and K. Iyakutti. Structural stability, electronic structure and mechanical properties of 4d transition metal nitrides (tmn) (tm=ru, rh, pd). *Journal of Physics and Chemistry of Solids*, 75(7):888 – 902, 2014.

[15]Alexey Kartsev and Nina Bondarenko. Thermodynamic Properties of NiAs-FeN Phase from First Principles. In *INTERNATIONAL CONFERENCE ON SIMULATION, MODELLING AND MATHEMATICAL STATISTICS (SMMS 2015)*, pages 423–427, 439 DUKE STREET, LANCASTER, PA 17602-4967 USA, 2015. Sci & Engn Res Ctr, DESTECH PUBLICATIONS, INC. International Conference on Simulation, Modelling and Mathematical Statistics (SMMS), Chiang Mai, THAILAND, NOV 22-23, 2015.

[16]Ken Niwa, Toshiki Terabe, Daiki Kato, Shin Takayama, Masahiko Kato, Kazuo Soda, and Masashi Hasegawa. Highly coordinated iron and cobalt nitrides synthesized at high pressures and high temperatures. *Inorganic Chemistry*, 56(11):6410–6418, 2017. PMID: 28509545.

[17]Dominique Laniel, Agnès Dewaele, Simone Anzellini, and Nicolas Guignot. Study of the iron nitride fen into the megabar regime. *Journal of Alloys and Compounds*, 733:53 – 58, 2018.

[18]Artem R. Oganov and Colin W. Glass. Crystal structure prediction using ab initio evolutionary techniques: Principles and applications. *The Journal of Chemical Physics*, 124(24):244704, 2006.

[19]Paolo Giannozzi, Stefano Baroni, Nicola Bonini, Matteo Calandra, Roberto Car, Carlo Cavazzoni, Davide Ceresoli, Guido L Chiarotti, Matteo Cococcioni, Ismaila Dabo, Andrea Dal Corso, Stefano de Gironcoli, Stefano Fabris, Guido Fratesi, Ralph Gebauer, Uwe Gerstmann, Christos Gougoussis, Anton Kokalj, Michele Lazzeri, Layla Martin-Samos, Nicola Marzari, Francesco Mauri, Riccardo Mazzarello, Stefano Paolini, Alfredo Pasquarello, Lorenzo Paulatto, Carlo Sbraccia, Sandro Scandolo, Gabriele Sclauzero, Ari P Seitsonen, Alexander Smogunov, Paolo Umari, and Renata M Wentzcovitch. Quantum espresso: a modular and open-source software project for quantum simulations of materials. *Journal of Physics: Condensed Matter*, 21(39):395502 (19pp), 2009.

[20]John P. Perdew, Kieron Burke, and Matthias Ernzerhof. Generalized gradient approximation made simple. *Phys. Rev. Lett.*, 77:3865–3868, Oct 1996.

[21]Hendrik J. Monkhorst and James D. Pack. Special points for brillouin-zone integrations. *Phys. Rev. B*, 13:5188–5192, Jun 1976.

[22]Nicola Marzari, David Vanderbilt, Alessandro De Vita, and M. C. Payne. Thermal contraction and disordering of the al(110) surface. *Phys. Rev. Lett.*, 82:3296–3299, Apr 1999.

[23]Stefan Maintz, Volker L Deringer, Andrei L Tchougréeff, and Richard Dronskowski. Lobster: A tool to extract chemical bonding from plane-wave based dft. *Journal of computational chemistry*, 37(11):1030–1035, 2016.

[24]Dario Alfè. Phon: A program to calculate phonons using the small displacement method. *Computer Physics Communications*, 180(12):2622–2633, 2009.

[25]Andriy O Lyakhov, Artem R Oganov, Harold T Stokes, and Qiang Zhu. New developments in evolutionary structure prediction algorithm uspex. *Computer Physics Communications*, 184(4):1172–1182, 2013.

[26]Colin W Glass, Artem R Oganov, and Nikolaus Hansen. Uspex—evolutionary crystal structure prediction. *Computer Physics Communications*, 175(11):713–720, 2006.

[27]Efficient iterative schemes for ab initio total-energy calculations using a plane-wave basis set.

[28]Matteo Cococcioni and Stefano de Gironcoli. Linear response approach to the calculation of the effective interaction parameters in the LDA + U method. *Phys. Rev. B*, 71:035105, Jan 2005.

[29]P. Asselin, R. F. L. Evans, J. Barker, R. W. Chantrell, R. Yanes, O. Chubykalo-Fesenko, D. Hinzke, and U. Nowak. Constrained monte carlo method and calculation of the temperature dependence of magnetic anisotropy. *Phys. Rev. B*, 82:054415, Aug 2010.

[30]R F L Evans, W J Fan, P Chureemart, T A Ostler, M O A Ellis, and R W Chantrell. Atomistic spin model simulations of magnetic nanomaterials. *Journal of Physics: Condensed Matter*, 26(10):103202, 2014.

[31]Haiyan Yan, Chunsheng Dou, Meiguang Zhang, and Hui Wang. Hexagonal high-pressure phase of tantalum mononitride predicted from first principles. *Journal of Applied Physics*, 113(8):083502, 2013.

[32]Jing Chang, Guo-Ping Zhao, Xiao-Lin Zhou, Ke Liu, and Lai-Yu Lu. Structure and mechanical properties of tantalum mononitride under high pressure: A first-principles study. *Journal of Applied Physics*, 112(8), 2012.

[33]H Nakagawa, S Nasu, H Fujii, M Takahashi, and F Kanamaru. 57fe mössbauer study of fen$_x$ (x = 0.25 - 0.91) alloys. *Hyperfine Interactions*, 69(1-4):455–458, 1992.

[34]X Wang, WT Zheng, HW Tian, SS Yu, W Xu, SH Meng, XD He, JC Han, CQ Sun, and BK Tay. Growth, structural, and magnetic properties of iron nitride thin films deposited by dc magnetron sputtering. *Applied surface science*, 220(1):30–39, 2003.

[35]L Rissanen, M Neubauer, K.P Lieb, and P Schaaf. The new cubic iron-nitride phase fen prepared by reactive magnetron sputtering. *Journal of Alloys and Compounds*, 274(1-2):74 – 82, 1998.

[36]K. Suzuki, H. Morita, T. Kaneko, H. Yoshida, and H. Fujimori. Crystal structure and magnetic properties of the compound fen. *Journal of Alloys and Compounds*, 201(12):11 – 16, 1993.

[37]E Bradley Easton, Th Buhrmester, and JR Dahn. Preparation and characterization of sputtered fe 1- x n x films. *Thin Solid Films*, 493(1):60–66, 2005.

[38]J-F Bobo, H Chatbi, M Vergnat, L Hennet, O Lenoble, Ph Bauer, and M Piecuch. Magnetic and structural properties of iron nitride thin films obtained by argon-nitrogen reactive

radio-frequency sputtering. *Journal of applied physics*, 77(10):5309–5313, 1995.

[39]Toru Hinomura and Saburo Nasu. 57fe mössbauer study of fen alloys. *Physica B: Condensed Matter*, 237-238:557 – 558, 1997. Proceedings of the Yamada Conference XLV, the International Conference on the Physics of Transition Metals.

[40]Zhonglong Zhao, Kuo Bao, Defang Duan, Fubo Tian, Bingbing Liu, and Tian Cui. Effects of magnetic ordering and electron correlations on the stability of fen. *RSC Adv.*, 5:31270–31274, 2015.

[41]A. Filippetti and W. E. Pickett. Prediction of a ferromagnetic ground state for nacl-type fen. *Phys. Rev. B*, 59:8397–8400, Apr 1999.

[42]Charles Kittel and Donald F Holcomb. Introduction to solid state physics. *American Journal of Physics*, 35(6):547–548, 1967.

[43]JiaoXi Yang, ZhiYong Xiao, ZiYang Li, Qiang Wen, and Feng Yang. First principles study on the structural, electronic and magnetic properties of ni4c. *Computational Condensed Matter*, 1:51 – 57, 2014.

[44]J Mathon. Pressure dependence of the magnetization in the itinerant electron model of ferromagnetism. *Journal of Physics F: Metal Physics*, 2(1):159, 1972.

[45]MSS Brooks and B Johansson. Exchange integral matrices and cohesive energies of transition metal atoms. *Journal of Physics F: Metal Physics*, 13(10):L197, 1983.

[46]Genrich L Krasko. Structural properties of bcc and fcc iron: Lmto-asa-stoner calculations. *Solid state communications*, 70(12):1099–1103, 1989.

[47]Stefano Baroni, Stefano de Gironcoli, Andrea Dal Corso, and Paolo Giannozzi. Phonons and related crystal properties from density-functional perturbation theory. *Rev. Mod. Phys.*, 73:515–562, Jul 2001.

[48]F. H. Herbstein and Jacques Smuts. Determination of debye temperature of α-iron by x-ray diffraction. *Philosophical Magazine*, 8(87):367–385, 1963.

[49]S.K. Sharma. Debye temperature of hcp iron at extreme compression. *Solid State Communications*, 149(47):2207 – 2209, 2009.

[50]B. Alling, T. Marten, and I. A. Abrikosov. Effect of magnetic disorder and strong electron correlations on the thermodynamics of crn. *Phys. Rev. B*, 2010.

[51]Liangcai Zhou, Fritz Körmann, David Holec, Matthias Bartosik, Blazej Grabowski, Jörg Neugebauer, and Paul H. Mayrhofer. Structural stability and thermodynamics of crn magnetic phases from *ab initio* calculations and experiment. *Phys. Rev. B*, 90:184102,

Nov 2014.

[52]J. A. Chan, Jefferson Z. Liu, Hannes Raebiger, Stephan Lany, and Alex Zunger. Relative stability, electronic structure, and magnetism of mnn and (ga,mn)n alloys. *Phys. Rev. B*, 78:184109, Nov 2008.

[53]Burak Himmetoglu, Andrea Floris, Stefano de Gironcoli, and Matteo Cococcioni. Hubbard-corrected dft energy functionals: The lda+u description of correlated systems. *International Journal of Quantum Chemistry*, 114(1):14–49, 2014.

[54]Polesya Svitlana, Kuhn Gerhard, Benea Diana, Mankovsky Sergiy, and Ebert Hubert. Electronic structure and magnetic properties of chromium chalcogenides and pnictides with nias structure. *Zeitschrift für anorganische und allgemeine Chemie*, 639(15):2826–2835.

[55]Anupam Roy, Samaresh Guchhait, Rik Dey, Tanmoy Pramanik, Cheng-Chih Hsieh, Amritesh Rai, and Sanjay K Banerjee. Perpendicular magnetic anisotropy and spin glass-like behavior in molecular beam epitaxy grown chromium telluride thin films. *ACS Nano*, 9(4):3772–3779, 2015. PMID: 25848950.

[56]K Komędera, AK Jasek, A Błachowski, K Ruebenbauer, and Anna Krztoń-Maziopa. Magnetic anisotropy in fesb studied by 57fe mössbauer spectroscopy. *Journal of Magnetism and Magnetic Materials*, 399:221–227, 2016.

[57]A. V. Ruban, A. B. Belonoshko, and N. V. Skorodumova. Impact of magnetism on fe under earth's core conditions. *Phys. Rev. B*, 87:014405, Jan 2013.

[58]A. A. Sorokin, S. V. Makogonov, and S. P. Korolev. The information infrastructure for collective scientific work in the far east of russia. *Scientific and Technical Information Processing*, 44(4):302–304, Oct 2017.

Stability and magnetism of FeN high-pressure phase with a NiAs-type structure.

Supplement materials.

Alexey Kartsev

Computing Center FEB RAS, Khabarovsk, Russia

School of Mathematics and Physics, Queens University Belfast,

Belfast BT7 1NN, northern Ireland, United Kingdom and

National Research Tomsk State University, 36, Lenina pr., Tomsk, 634050, Russia.

Oleg Feya

Moscow Institute of Physics and Technology,

Dolgoprudny, Moscow Region 141700, Russia

Nina Bondarenko

Condensed Matter Theory Group, Physics Department,

Uppsala University, S-751 21 Uppsala, Sweden

Alexander G. Kvashnin

Moscow Institute of Physics and Technology,

Dolgoprudny, Moscow Region 141700, Russia and

Skolkovo Institute of Science and Technology, 3 Nobel St., Moscow 143026, Russia

Artem R. Oganov

Moscow Institute of Physics and Technology,

Dolgoprudny, Moscow Region 141700, Russia

Department of Geosciences, Center for Materials by Design,

and Institute for Advanced Computational Science,

Stony Brook University, Stony Brook, New York 11794, USA

Skolkovo Institute of Science and Technology,

3 Nobel St., Moscow 143026, Russia and

School of Materials Science, Northwestern Polytechnical University, Xi'an 710072, China

(Dated: July 19, 2022)

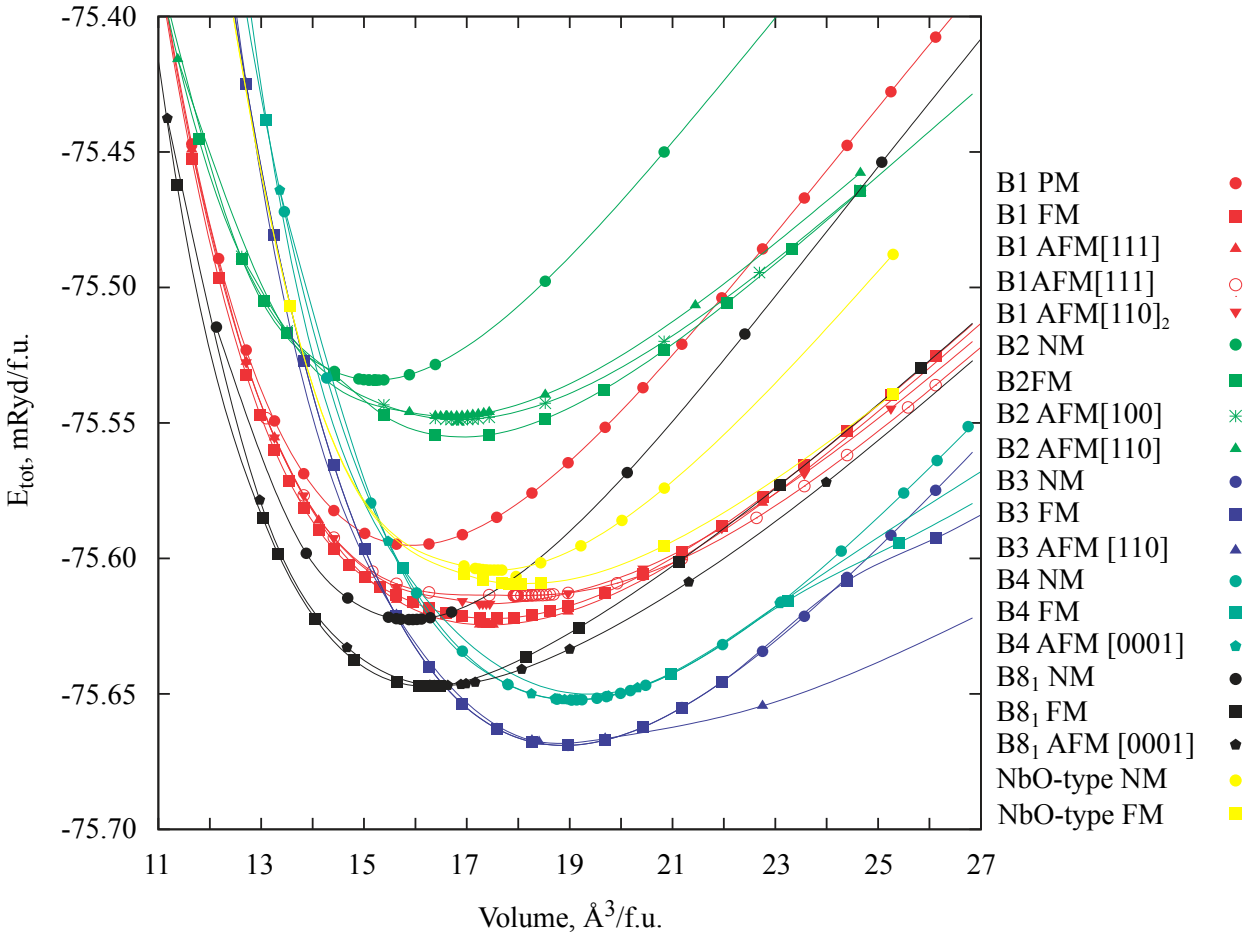

FIG. 1. Total energy versus elementary volume per formula unit for different FeN phases in various magnetic states - nonmagnetic (NM), ferromagnetic (FM) and antiferomagnetic (AFM).

I. TOTAL ENERGY CALCULATIONS FOR ALL FEN PHASES.

It is clearly seen from the Fig. 1 that the NM ZnS FeN phase has the lowest total energy among others at equilibrium and can be transformed to FM NiAs FeN under pressure.

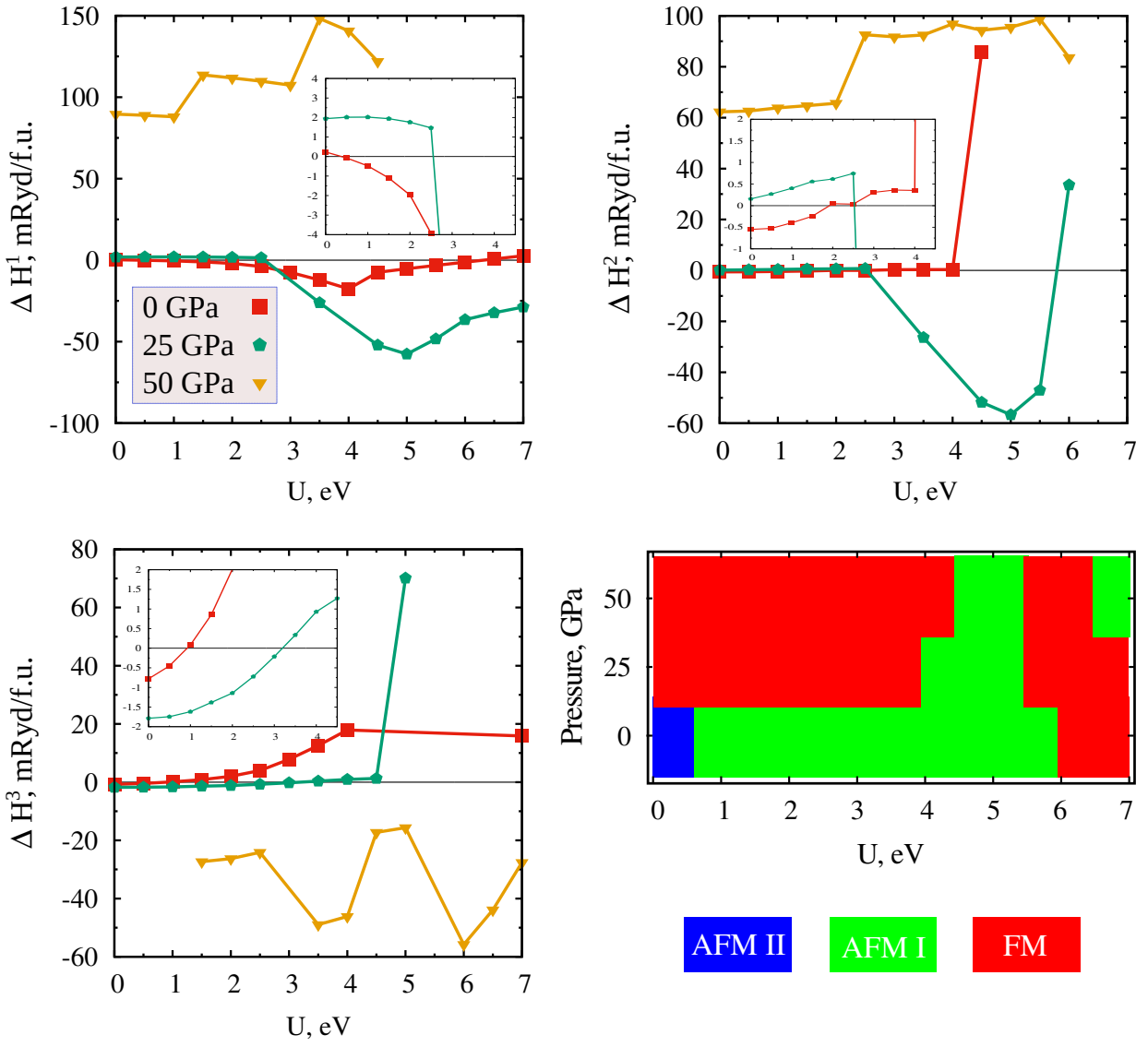

FIG. 2. Enthalpies differences per formula unit between ferromagnetic (FM) and antiferomagnetic (AFM [0001] and AFM $[0001]_2$) configurations as a function of on-site Hubbard interaction U applied to d-orbitals of iron atoms at different pressure. where $\Delta H^1 = H(AFM[0001]_1) - H(FM)$, $\Delta H^2 = H(AFM[0001]_2) - H(FM)$ and $\Delta H^3 = H(AFM[0001]_2) - H(AFM[0001]_1)$. The inserts are zoomed graphs for 0-4.5 eV range of U values. The absence of some data points is due to the convergence problems during the self-consistent calculations.

II. ENTHALPIES DIFFERENCES FOR THE COMPETITION BETWEEN OF THE FM, AFM [0001] AND AFM$[0001]_2$ SPIN ARRANGEMENT IN THE MAGNETIC B8_1.

Enthalpies differences and stability diagram for FM, AFM [0001] and AFM$[0001]_2$ spin arrangements in the relaxed magnetic B8_1 phase has been computed as a function of on-site Hubbard U

intercalation for three different values of external pressure - 0, 25 and 50 GPa (see Fig. 2). The AFM$[0001]_2$ configuration is found to be most favourable for all $U \lesssim 0.5$ eV at 0 GPa external pressures, while the FM configuration is more preferable than AFM phases for all $U \lesssim 4.5$ eV for at 25 GPa and 50 GPa pressures. The rest of the diagram has more complicated character and indicate the interplay between FM and AFM exchanges in the magnetic $B8_1$ phase to be sensitive on the Hubbard U and external pressure.

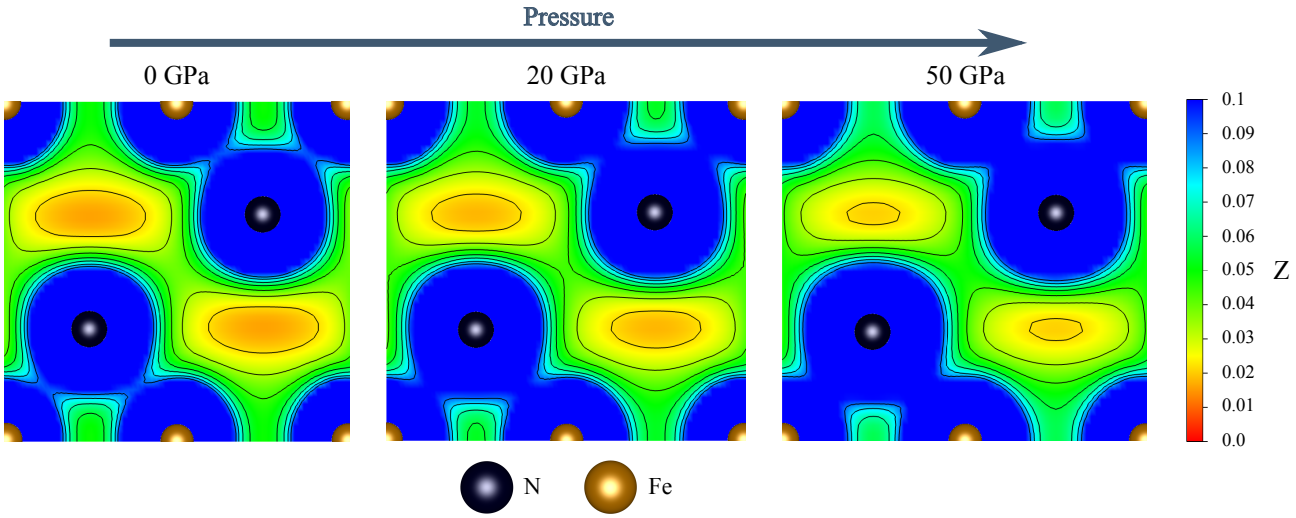

FIG. 3. 2D charge density map evolution during external pressure increasing. The shown charge density map ($0 < Z < 0.1\ e/Bohr^3$) correspond to the (012) plane of the primitive $B8_1$ FeN phase cell. Covalent interaction between Fe and N atoms is clearly visible from the localized valence electrons between the Fe and N atoms and become slightly stronger with pressure.

III. CHARGE DENSITY AND COVALENT BONDINGS UNDER THE EXTERNAL PRESSURE.

The charge density map plotted in Fig. 3 confirm the strong covalent characteristics of NiAs FeN. The Fe-N covalent bonding in this phase become stronger with pressure.

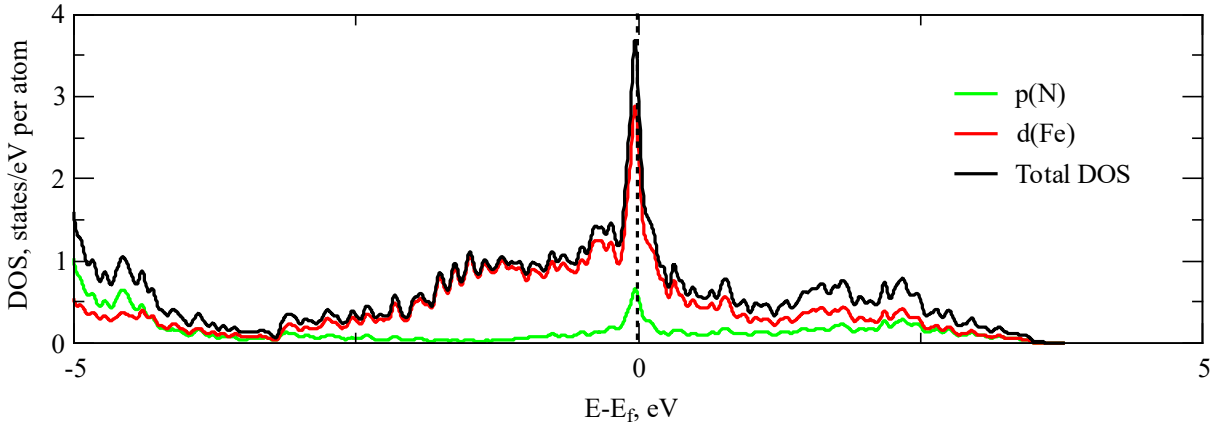

FIG. 4. Density of states and partial density of states for non-magnetic $B8_1$ FeN phase. Red curve is d-orbitals contribution of Fe atoms and green curve is p-orbitals contribution from nitrogen atoms.

IV. STONER CRITERIA AND NON-MAGNETIC $B8_1$ FEN PHASE

Due to the $p(N) - d(Fe)$ orbitals hybridization, the larger value of DOS at Fermi level $N(E_F)$ together with a band widening emerge at the electronic structure of NM $B8_1$ FeN phase. So $1/N(E_F) >> W$ show that interaction energy is rather higher them the kinetic energy, and thereby favor ferromagnetism and make non-magnetic state unstable.

V. COHP CALCULATION

The Hamilton-weighted populations were calculated based on periodic plane-wave density-functional theory output with the aid of the Local-Orbital Basis Suite Towards Electronic-Structure Reconstruction software package 'LOBSTER'[1]. With a COHP analysis, it is possible to determine the strength of Fe-N and Fe-Fe bonds of different phases and to understand the bond changes under pressure and during the phase transition. Since $Fe\uparrow - Fe\downarrow$ bonding of the first coordinate sphere always falls into antibonding regions the AFM coupling is less strength than FM. It is clear that the -ICOHP bond strength of $Fe-Fe$ bonds for DOWN-spin channel is higher for FM coupling than for AFM, while the UP-channel is stronger for AFM $Fe-Fe$ bonding. The ICOHP of $N-N$ is almost independent from the spin arrangement in the FeN structure. Looking to the occupied valence regions of all magnetic FeN structures one can notice a heavy domination of the p nitrogen levels in a broad energy region which confirms once again the strong covalency of magnetic FeN.

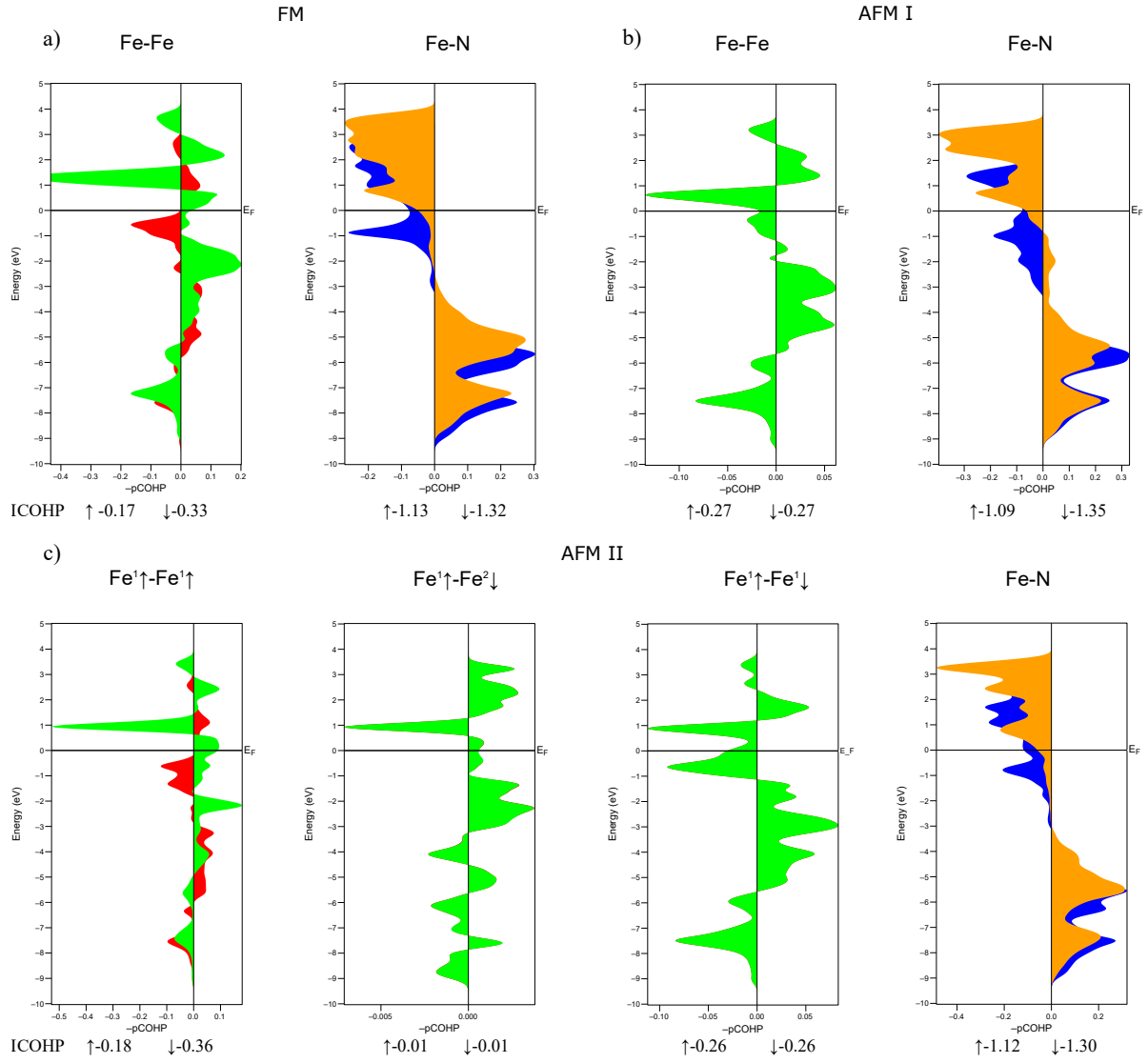

FIG. 5. Calculated crystal orbital Hamilton population (-COHP) for bonding analyses of (a) FM, (b) AFM I (AFM$[0001]_1$) and (c) AFM II (AFM$[0001]_2$) $B8_1$ FeN phases - for UP ↑ and DOWN ↓ spin channels separately. Green and red color indicate UP and DOWN spin respectively for $Fe-Fe$ bonding of the first coordinate sphere (for AFM I structure it correspond to the oppositely polarized iron atoms). Blue and tuscany colour indicate UP and DOWN spin channel respectively for $Fe-N$ bonding of the first coordinate sphere. The horizontal line represents the Fermi level E_F, which is shifted so that it equal to zero. $\uparrow-\uparrow$ and $\uparrow-\downarrow$ correspond to the same and oppositely polarized iron atoms and Fe^1-Fe^1 and Fe^1-Fe^2 bondings correspond to iron-iron interaction in the first and second coordinate sphere respectively for the AFM II structure. ICOHP is the integrated -COHP up to the Fermi level for each spin separately. Notice that for $\uparrow-\downarrow$ bonding UP and DOWN COHPs are equal, thereby green and red colours are superimposed on each other for AFM bondings.

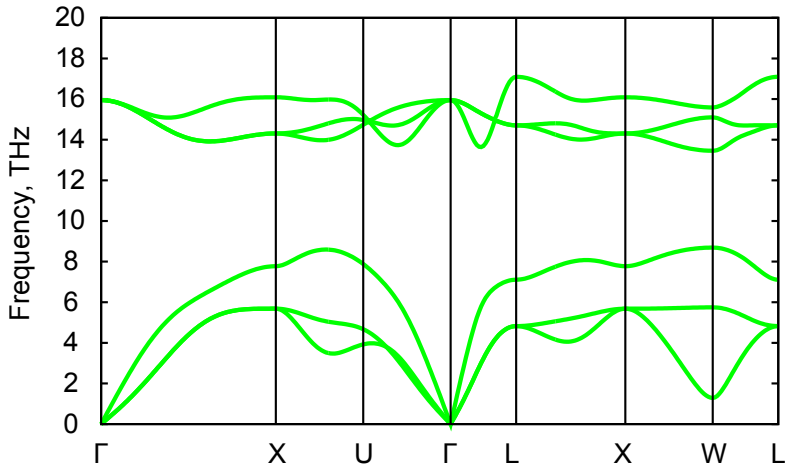

FIG. 6. Phonon spectra for nonmagnetic B3 FeN at the experimental lattice parameter a_{B3}^{exp} =4.335 Å[2].

VI. DYNAMIC STABILITY OF GROUND STATE FEN PHASE AT ZERO PRESSURE - NM B3 FEN STRUCTURE.

The absence of imaginary modes in phonon spectra for NM B3 FeN phase reveal its stability at experimental lattice parameter a_{B3}^{exp} =4.335 Å.

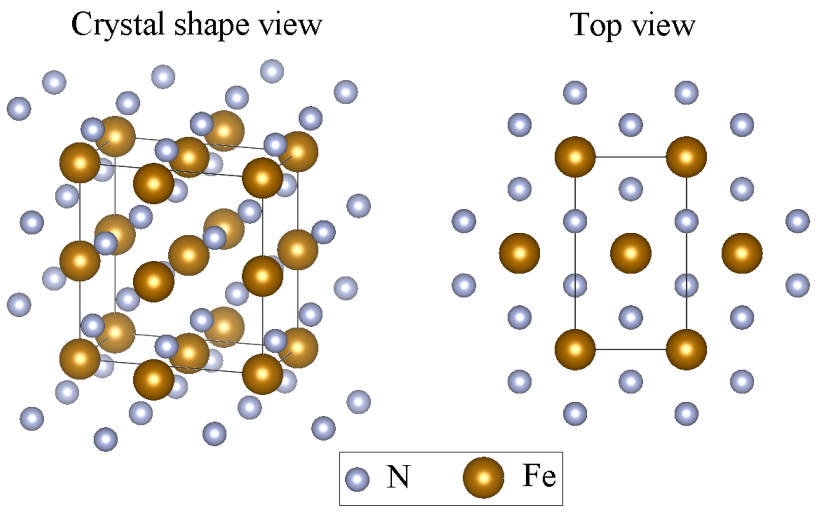

FIG. 7. Rectangular unit cell of FM $B8_1$ structure used for magnetic exchange calculation.

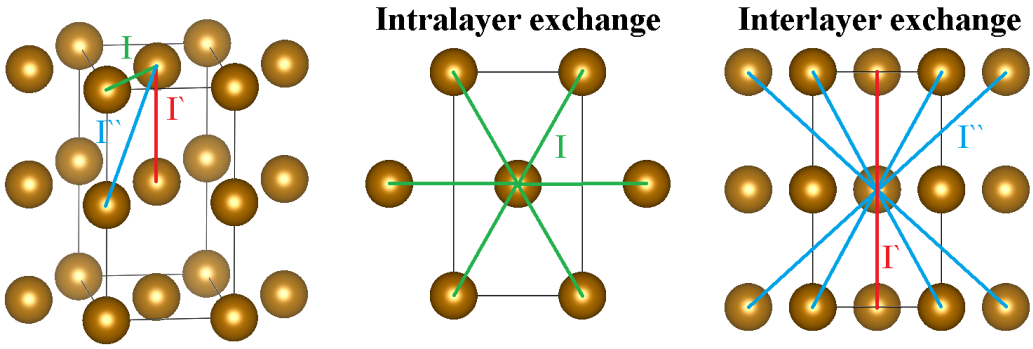

FIG. 8. Intra-layer and inter-layer exchange scheme in the proposed rectangular unit cell of FM $B8_1$ structure which correspond to magnetic iron sublattice.

A. Critical temperature calculation for FM $B8_1$ FeN phase.

In order to describe magnetic properties of FM $B8_1$ FeN we consider here Heisenberg model with an isotropic exchange for one type of the intra-layer first nearest neighbour exchange (exchange inside hexagonal layers of NiAs-type structure) and two types of the first I' and the second I'' inter-layer nearest neighbour exchanges:

$$H = \sum_{<i,j>} I\vec{S}_i\vec{S}_j + \sum_{<i,j>\prime} I'\vec{S}_i\vec{S}_j + \sum_{<i,j>\prime\prime} I''S_iS_j, \tag{1}$$

where $\vec{S}_i$ and $\vec{S}_j$ are directions of magnetic moments on the i and j metal atoms respectively.

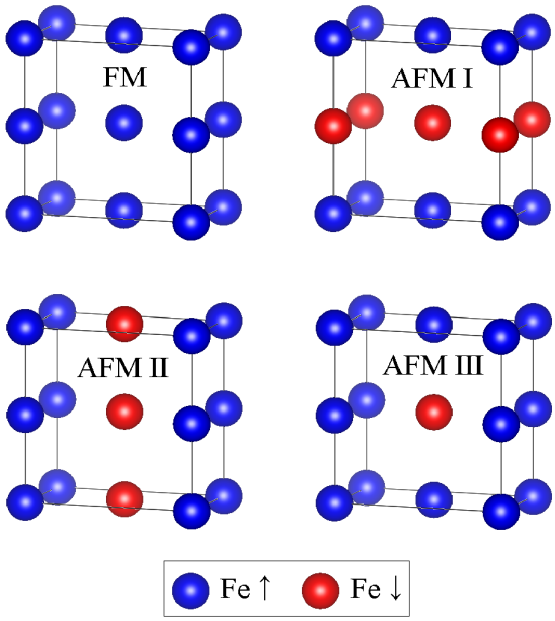

FIG. 9. Four different magnetic configurations used for magnetic exchange calculation between Fe atoms in the framework of DFT: ferromagnetic (FM) and three different anti-ferromagnetic configurations (AFM I, AFM III, AFM III).

Since magnetic Fe atoms of $B8_1$ structure forms a hexagonal sublattice, in order to implement proposed nearest-neighbor interactions we have to consider an orthorhombic unit cell containing 4 atoms of Fe (see Fig. 7). Therefore using this unit cell magnetic exchanges I, I' and I'' between Fe atoms can be consider in the frame of DFT calculations along with the crystal translation invariance (see Fig. 8).

By performing the DFT calculations for a crystal with different spin configurations of the magnetic sublattice one can map it onto the model system. Since we do not consider any type of anisotropy we can stick to collinear DFT calculations for four different unique collinear spin configurations (see Fig. 9): FM - where all the spins allies along the same spin-up direction, AFM I - where one by one hexagonal layers along the z-direction are oppositely polarized, AFM II - where all the hexagonal layers are identical and 2 atoms are oppositely polarized in each layer of the unit cell, and AFM III - where the only atom in the center of the unit cell has spin-down polarization oppositely to the rest of atoms. Based on the model proposed the following relations of total energies per unit cell for above configurations can be derived:

$$E_{FM} = 24I + 8I' + 48I'' \tag{2}$$

$$E_{AFMI} = 24I - 8I' - 48I'' \tag{3}$$

$$E_{AFMII} = -8I + 8I' - 16I'' \tag{4}$$

$$E_{AFMIII} = 8I \tag{5}$$

$$\tag{6}$$

Since in the framework of DFT the absolute value of total energies has no physical meaning, we have to use the difference between them. So one can take the ferromagnetic state as a reference point and subtract it from other relations. Thereby we can map our model onto DFT results using following relations:

$$\Delta E_{AFMI} = E_{AFMI} - E_{FM} = -16I' - 96I'' \tag{7}$$

$$\Delta E_{AFMII} = E_{AFMII} - E_{FM} = -32I - 64I'' \tag{8}$$

$$\Delta E_{AFMIII} = E_{AFMIII} - E_{FM} = -16I - 8I' - 48I'' \tag{9}$$

By solving this system of linear equations we can get the following unique solution for values of exchange parameters:

$$I = (\Delta E_{AFMI} - 2\Delta E_{AFMIII})/32 \tag{10}$$

$$I' = (-6\Delta E_{AFMIII} + 3\Delta E_{AFMII} + \Delta E_{AFMI})/32 \tag{11}$$

$$I'' = -(-2\Delta E_{AFMIII} + \Delta E_{AFMII} + \Delta E_{AFMI})/64 \tag{12}$$

For DFT GGA+U calculations with $U > 0$ eV obtained exchange parameters are lower, thereby it will lower the calculated T_C value. While using the same formalism for relaxed AFM [0001] structure we computed exchange parameters and got following numbers: $I = -16.5888$ meV, $I' = -0.4334$ meV and $I'' = -0.4007$ meV. Thereby it clear identify the preference of the ferromagnetic order in comparison to AFM [0001] spin arrangement for magnetic $B8_1$ FeN phase and $U = 0$ eV.

Based on the proposed model we performed Mote Carlo simulations[3] in "Vampire" atomistic spin dynamics program[4]. A 50×50×50 model super-cell with periodic boundary conditions and 32,000 sites was used.

U, eV	δE^1	δE^2	δE^3	Favourable direction
0	2.69	2.63	-0.06	$[11\bar{2}0]$
1	3.36	3.04	-0.32	$[11\bar{2}0]$
2	10.45	9.08	-1.37	$[11\bar{2}0]$
3	2.76	2.94	0.19	$[1\bar{1}00]$
4	-0.64	7.29373	7.93256	$[1\bar{1}00]$

TABLE I. Magnetic anisotropy at zero pressure as a function of on-site Hubbard U. $\delta E^1 = E[0001] - E[11\bar{2}0]$ $\delta E^2 = E[0001] - E[1\bar{1}00]$ $\delta E^3 = E[11\bar{2}0] - E[1\bar{1}00]$

VII. MAGNETIC ANISOTROPY AND EXCHANGES AT ZERO PRESSURE AS A FUNCTION OF ON-SITE HUBBARD U.

Using non-collinear calculations the magnetic anisotropy energy (MAE) for FM $B8_1$ FeN phase along three different directions ([0001], $[11\bar{2}0]$ and $[1\bar{1}00]$) has been computed using the rectangular unit cell. Each magnetic configuration has been relaxed at each U value and zero pressure. Results clearly indicate the switch of easy-direction for $U \gtrsim 2$ eV which indicate a complicated behaviour of MAE as a function of U direction therefore can suggest the non-collinear frustrated in-plane configuration.

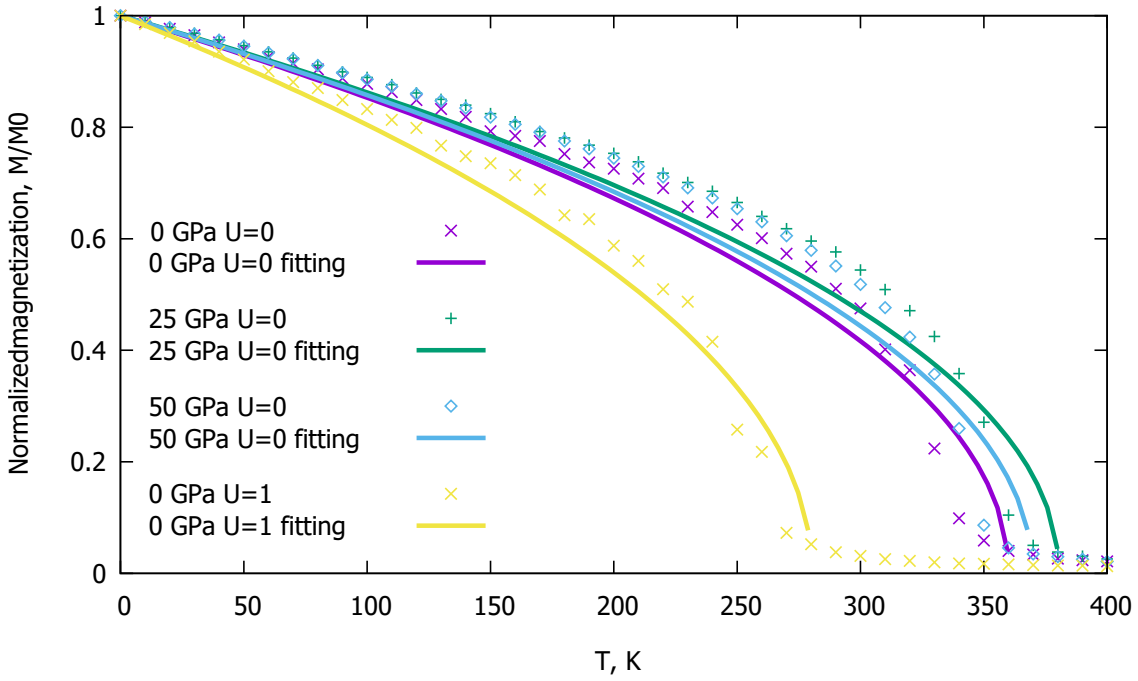

FIG. 10. Monte Carlo simulation of temperature-dependent magnetization for FM $B8_1$ FeN phase at different pressures and for on-site Hubbard $U = 1$ eV at 0 GPa (shown by dots). The temperature-dependent magnetization is fitted to the expression $M^f(T)/M_0 = (1 - T/T_c)^\beta$ (shown by solid lines).

U, eV	P, GPa	I, meV	I', meV	I'', meV	T_c, K
0	0	-22.17	-16.35	2.24	360
0	25	-21.08	-17.20	1.91	380
0	50	-19.43	-17.51	1.72	370
1	0	-18.52	7.95	-1.52	280
2	0	-20.64	14.96	-1.86	0
3	0	-12.08	43.86	-1.72	0
4	0	101.05	104.75	-44.01	0

TABLE II. Magnetic exchanges at different pressures and for different on-site Hubbard U values.

VIII. MAGNETIC EXCHANGES AND CURIE TEMPERATURE AT DIFFERENT PRESSURES AND FOR DIFFERENT ON-SITE HUBBARD U VALUES.

Magnetic exchanges I, I' and I'' have been obtained using the collinear spin-polarized calculations for relaxed structures of FM $B8_1$ FeN phase at each U value. Zero values of T_c mean that structure has spin coupling where the anti-ferromagnetic exchange is dominant, and thereby do not exhibit total magnetization at any temperature.

[1] Stefan Maintz, Volker L Deringer, Andrei L Tchougréeff, and Richard Dronskowski. Lobster: A tool to extract chemical bonding from plane-wave based dft. *Journal of computational chemistry*, 37(11):1030–1035, 2016.

[2] L Rissanen, M Neubauer, KP Lieb, and P Schaaf. The new cubic iron-nitride phase fen prepared by reactive magnetron sputtering. *Journal of alloys and compounds*, 274(1-2):74–82, 1998.

[3] P. Asselin, R. F. L. Evans, J. Barker, R. W. Chantrell, R. Yanes, O. Chubykalo-Fesenko, D. Hinzke, and U. Nowak. Constrained monte carlo method and calculation of the temperature dependence of magnetic anisotropy. *Phys. Rev. B*, 82:054415, Aug 2010.

[4] R F L Evans, W J Fan, P Chureemart, T A Ostler, M O A Ellis, and R W Chantrell. Atomistic spin model simulations of magnetic nanomaterials. *Journal of Physics: Condensed Matter*, 26(10):103202, 2014.